Synthesis of isomeric β-cycloalkoxyphosphonated hydrazones containing a dioxaphosphorinane ring: Configurational and conformational investigation and molecular docking analysis

Dorra Kanzari-Mnallah, Sirine Salhi, Michael Knorr, Jan-Lukas Kirchhoff, Carsten Strohmann, Med Lotfi Efrit, Azaiez Ben Akacha

Journal of Molecular Structure 1317 (2024) 139035

Contents lists available at ScienceDirect

Journal of Molecular Structure

journal homepage: www.elsevier.com/locate/molstr

Synthesis of isomeric β-cycloalkoxyphosphonated hydrazones containing a dioxaphosphorinane ring: Configurational and conformational investigation and molecular docking analysis

Dorra Kanzari-Mnallah [a,*], Sirine Salhi [a], Michael Knorr [b,*], Jan-Lukas Kirchhoff [c], Carsten Strohmann [c], Med Lotfi Efrit [a], Azaiez Ben Akacha [a]

[a] Laboratory of Selective Organic and Heterocyclic Synthesis-Biological Activity Evaluation, SOHES, (LR17ES01), Department of Chemistry, Faculty of Science of Tunis, University Tunis El Manar 2092 Tunis Tunisia
[b] Institut UTINAM-UMR CNRS 6213, Université de Franche-Comté, 16, route de Gray 25030 Besançon, France
[c] Anorganische Chemie, Technische Universität Dortmund, Otto-Hahn-Str. 6 44227 Dortmund, Germany

ARTICLE INFO

Keywords:
Allenylphosphonate
Hydrazone
Dioxaphosphorinane
Azine
Conformers, ^{31}P NMR
DFT calculation
SCXRD
Molecular Docking
ADMET

ABSTRACT

A series of *Z/E* isomeric β-cycloalkoxyphosphonated hydrazones [$R^1R^2C(CH_2O)_2P(=O)CH2\text{-}C\{=N—N(H)R^5\}C(H)R^3R^4$] **3** bearing a six-membered dioxaphosphorinane ring was prepared, structurally analysed, and subjected to *in silico* studies to assess their Acetylcholinesterase (AChE) and Butyrylcholinesterase (BuChE) inhibition activity. Furthermore, their ADMET (Absorption, Distribution, Metabolism, Excretion, Toxicity) properties were determined. Hydrazones **3** were prepared from their corresponding allenylphosphonates [$R^1R^2C(CH_2O)_2P(=O)C(H)=C=CR^3R^4$] **2** by addition of various hydrazines NH_2–NHR^5. Since NMR studies indicated the occurrence of several isomeric species in solution, conformational and configurational studies, based on mechanistic elucidation and energy stability using Density functional theory (DFT) calculation at the B3LYP/6-311 *G*++ (d,p) level of theory, were performed to determine their relative predominance. The hydrazone 1-(2-oxo-1,3,2-dioxaphosphoranyl)-3-phenylpropanone **3c** was crystallographically analysed by single-crystal X-ray diffraction (SCXRD), revealing the occurrence of strong intra- and intermolecular N—H···O hydrogen bonding. These secondary interactions were further examined by a Hirshfeld surface analysis. The experimental SCXRD parameters are compared with the theoretical calculated ones and the preferred configuration of product **3c** was determined. Furthermore, the crystal structure of the symmetric azine 2,2′-((2*E*,2′*E*)-hydrazine-1,2-diylidenebis(3-phenylpropan-1-yl-2-ylidene))bis(5-methyl-5-propyl-1,3,2-dioxaphosphinane 2-oxide) **4**, resulting from the reaction between hydrazone **3a** and allene **2a**, has been determined. To predict whether hydrazones **3** are appropriate as anticholinesterase agents exhibiting a potential activity for treatment of the Alzheimer disease, *in silico* molecular docking simulations were employed to investigate the interaction modes between hydrazones **3** and the active sites of the BuChE and AChE enzymes. Additionally, an ADMET-properties prediction was carried out for selected hydrazones to determine their pharmacokinetics and drug-likeness properties.

1. Introduction

Hydrazones derivatives featuring the motif R_1R_2C=N-N(H)R_3 (R = H, alkyl, aryl) represent attractive targets that continue to receive attention due to their significant biological and therapeutic properties [1]. The presence of an imine-type C═N function makes them also interesting as *N*-donor ligand in coordination chemistry [2-4]. Some representatives of this class display also important biological activities such as analgesic [5,6], anti-microbial [7], anti-cancer [8-11], anti-convulsant [12], anti-inflammatory [13] properties. Previous studies [14-16] have also revealed that some hydrazone derivatives may have a significant inhibitory activity against Butyrylcholinesterase (BuChE) and/or Acetylcholinesterase (AChE) (Fig. 1).

BuChE and AChE are enzymes involved in Acetylcholine (ACh = 2-acetoxyethyl-trimethylammonium) hydrolysis yielding the inactive metabolites choline and acetate. ACh is an important neurotransmitter for the regulation of cognition in humans and the activation of muscles. Cholinesterase inhibitors (https://en.wikipedia.org/wiki/Acetylcholi

* Corresponding author.
E-mail address: michael.knorr@univ-fcomte.fr (M. Knorr).

https://doi.org/10.1016/j.molstruc.2024.139035
Received 24 February 2024; Received in revised form 26 May 2024; Accepted 13 June 2024
Available online 22 June 2024

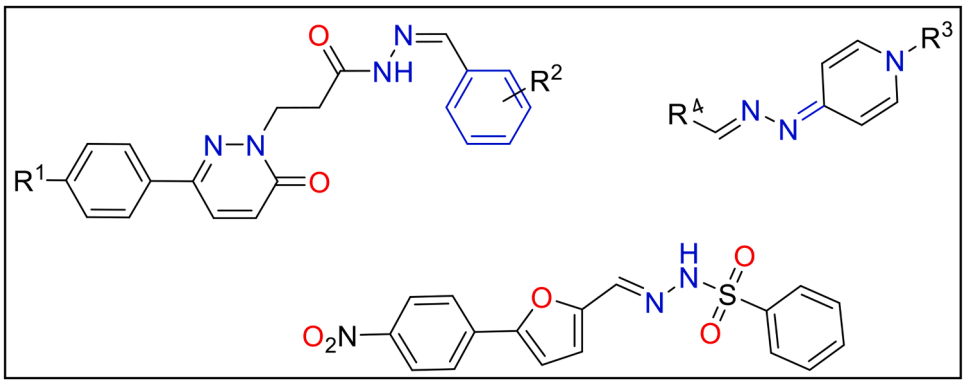

Fig. 1. Examples of previously reported hydrazones [14-16] featuring significant inhibitory activity against BuChE and/or AChE.

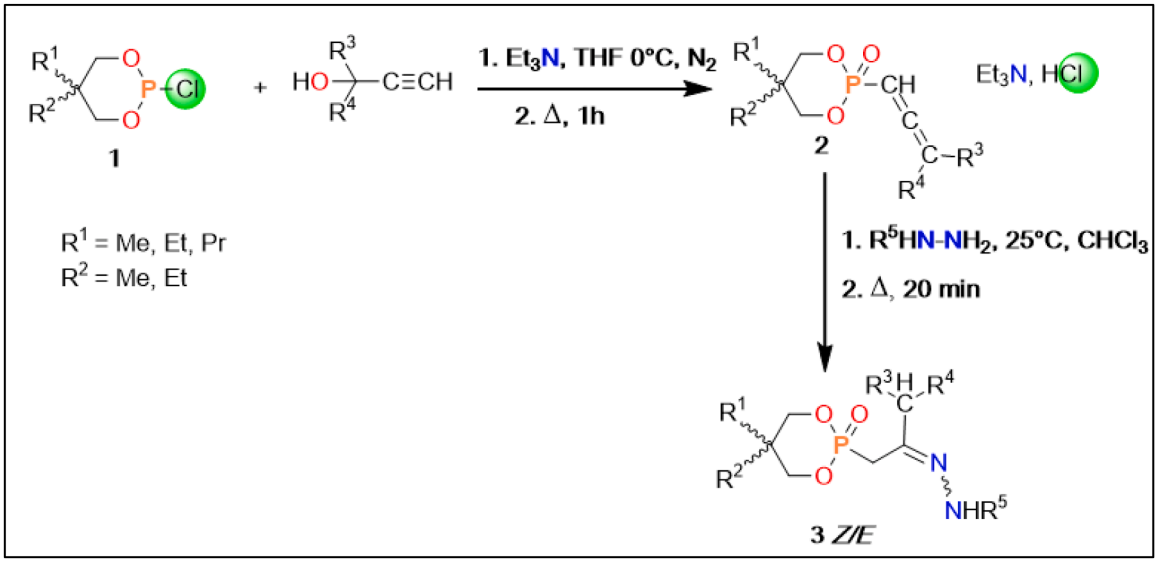

Scheme 1. Synthetic pathway leading to allenes **2** and hydrazones **3**.

nesterase inhibitor) are employed for the treatment of the Alzheimer disease [17-19]. Despite all the progress and discoveries made for treatment of this neurodegenerative disease, further research is needed to enlarge the library of more effective agents. Consequently, synthesizing new molecules whose structural motifs are close to that of chemical entities having proven activity and assessing whether they present potential activity, remains a challenge.

In this context, a series of hydrazones [$R^1R^2C(CH_2O)_2P(=O)CH_2$-C{=N-N(H)$R^5$}C(H)$R^3R^4$] **3** bearing a six-membered 1,3,2-dioxaphosphorinane heterocycle was synthesised from their corresponding phosphonated allenes **2** and obtained as diastereomeric product mixtures. With the aim to determine the predominant configurations of the diastereomeric allene [Me(Pr)$C(CH_2O)_2P(=O)C(H)=C=C(H)Ph$] **2a** and its derived diastereomeric hydrazone **3a**, a computational method was used. In addition, the structural characterisation of a single crystal of hydrazone **3c** by X-Ray diffraction is reported in this paper. A DFT calculation allowed to investigate the geometrical properties and to compare them with the experimental data of the analyzed compound. With the intention to screen if the prepared hydrazones could be employed as potential candidates acting as AChE or BuChE inhibitors for use in the treatment of Alzheimer disease, an *in silico* simulation was performed. To analyse any secondary interactions and bonding modes occurring between the β-cycloalkoxyphosphonated hydrazones **3** and the active sites of the AChE and BuChE enzymes, a molecular docking study was conducted. To predict their pharmacokinetics and drug-likeness properties, an ADMET profile was established for some selected hydrazones.

Table 1
Substitution pattern, yield and $^{31}P\{^1H\}$ NMR data of allenes **2a-e**.

2	a	b	c	d	e	f
R^1	Me	H	H	Me	Et	Et
R^2	Pr	H	H	Me	Et	Et
R^3	H	Me	Me	H	H	Me
R^4	Ph	Me	Ph	Ph	Ph	Me
Yield%	84	75	78	70	90	72
^{31}P NMR (ppm)	6.7; 7.4	9.6	7.6	6.5	7.4	11.2
	cis **/*trans*** **ratio** 27: 73					

2. Results and discussion

2.1. Chemistry

2.1.1. Preparation of allenylphosphonates *2a-e* and β-cycloalkoxyphosphonated hydrazones *3a-f*

In continuation of previous work published by our laboratory [20-23], a series of allenylphosphonates **2** was synthesised based on a method developed by Boiselle et al. (Scheme 1) [24-26]. The structural modifications concern substitutions of R^1 and R^2 on the dioxaphosphorinane ring. Also, R^3 and R^4 were modified owing the use of different

Table 2
Substitution pattern, yield, $^{31}P\{^{1}H\}$ NMR data and diastereomeric ratios of hydrazones **3a-f**.

3		a	b	c	d	e	f
R^1		Me	H	H	Me	Et	Et
R^2		Pr	H	H	Me	Et	Et
R^3		H	Me	Me	H	H	H
R^4		Ph	Me	Ph	Ph	Ph	Ph
R^5		H	H	H	H	H	Me
Yield%		74	80	75	70	70	80
^{31} P NMR (ppm)	$3a_1$ 21.12; 21.37;	$3a_2$ 21.69; 21.55	21.5; 21.4	20.8	20.9; 20.7	21.7; 21.9	21.8; 21.3
Z/E ratio	61: 39	57:43	96: 4	100:0	86: 14	62: 38	85: 15

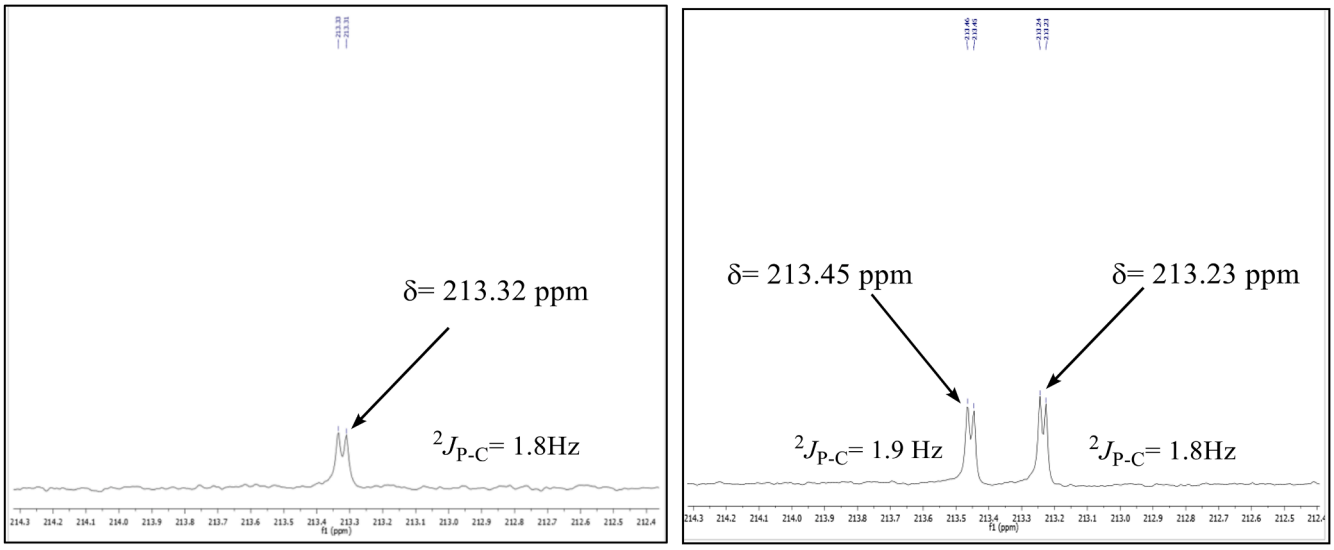

Fig. 2. Comparison of characteristic allenic carbon's signals of **2d** and **2a** in the ^{13} C NMR spectra. (left) Part of the $^{13}C\{^{1}H\}$ NMR spectrum **2d**. (right) Part of $^{13}C\{^{1}H\}$ NMR spectrum of allene **2a.**

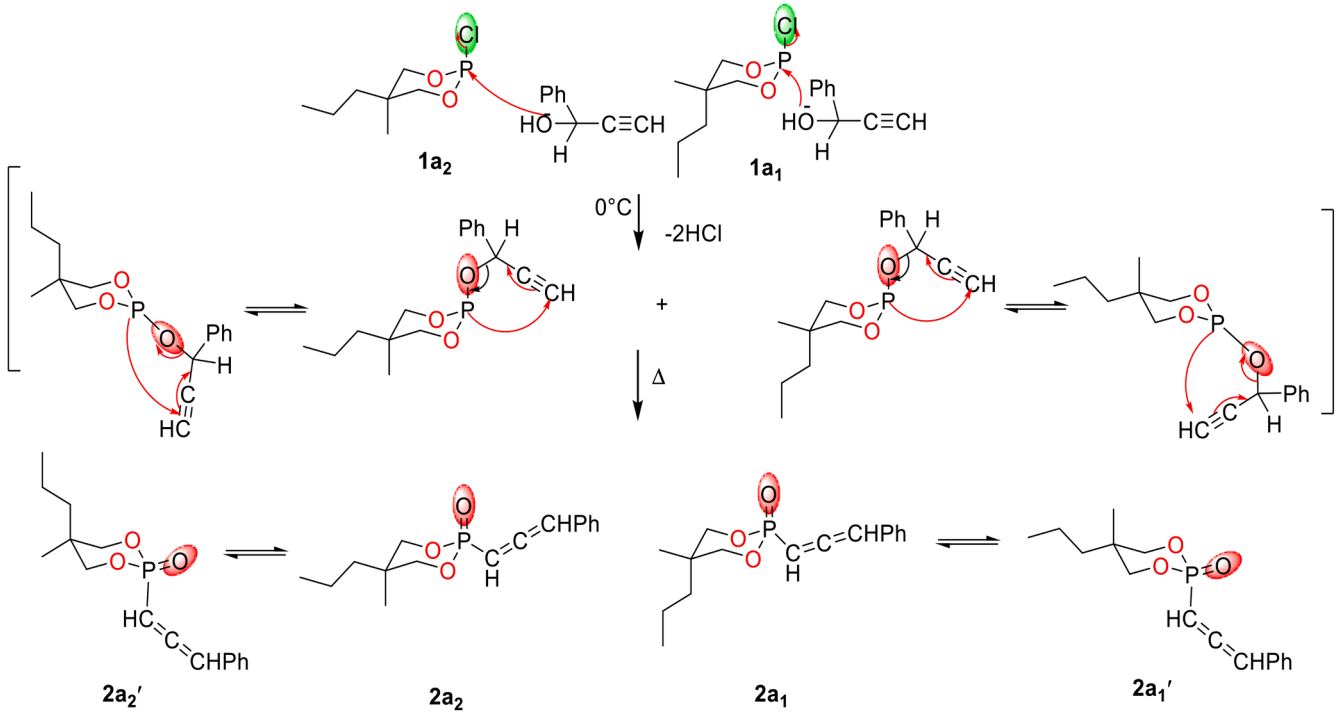

Scheme 2. Proposed mechanism for the formation of **2a.**

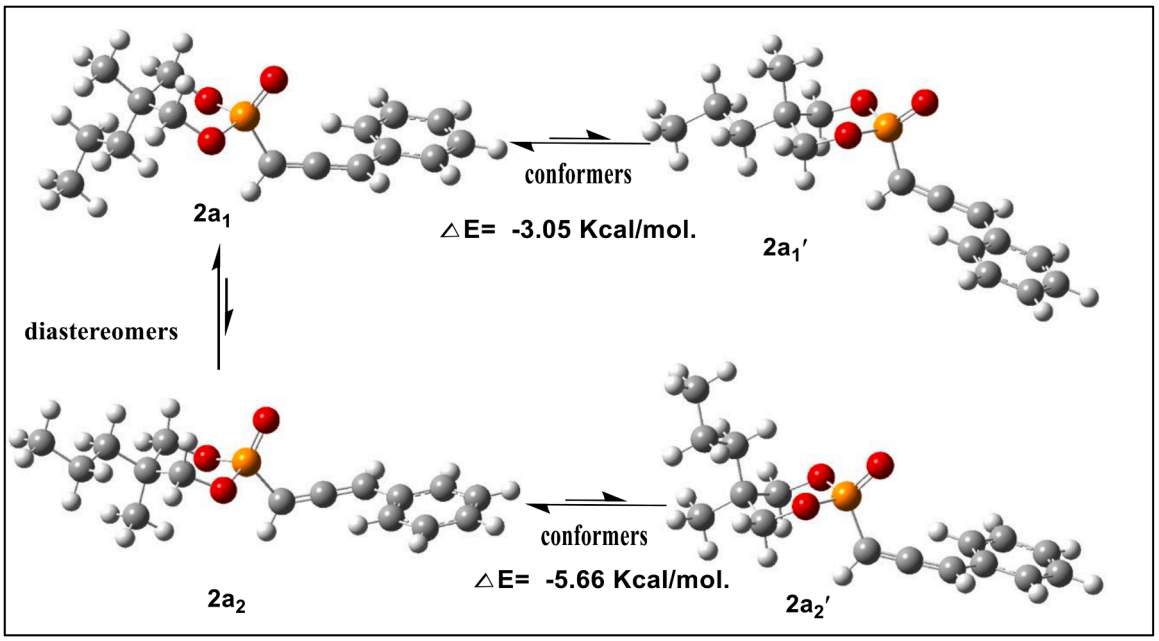

Fig. 3. Computed preferred conformations for conformers **2a$_1$, 2a$_1$'; 2a$_2$, 2a$_2$'**.

propargylic alcohols. The first step in the synthetic pathway involves the addition of propargylic alcohol to 2-chloro-5,5-dialkyldioxaphosphorinane **1** in an equimolar quantity at 0 °C using an anhydrous solvent, in the presence of triethylamine as an additional base. The allenylphosphonates **2** were thus prepared in high yield varying from 72 % to 90 % and were isolated as white solids (Table 1). To convert them into the corresponding hydrazones **3**, the respective hydrazines were added at room temperature. After heating the mixture for 40 min, the targeted hydrazones **3** were isolated in good yields ranging from 70 % to 80 % (Scheme 1 and Table 2). All prepared hydrazones were collected as white solids, except for **3b,** which has a pasty consistency.

*2.1.2. Spectroscopic characterisation and mechanistic elucidation of **2a**.*

In the proton-decoupled ^{31}P NMR spectrum of allene **2a**, two signals are observed at 6.7 and 7.4 ppm, whereas for the other products **2b-f**, only a single resonance appears in the range between 6.5–10.75 ppm (Table 1). This indicates that allene **2a** (in which the dioxaphosphorinane ring substituents $R^1 \neq R^2$), exists as a mixture of two diastereomers. This is confirmed by the duplication of the doublet resonance (due to $^2J_{P\text{-}C}$ coupling) characteristic of the allenic carbon =C= in the $^{13}C\{^1H\}$ NMR spectrum of **2a**, which is absent in that of **2d** (where $R^1 = R^2$) (Fig. 2).

A mechanistical proposal for the formation of **2a** is depicted in Scheme 2. The reaction begins with a nucleophilic attack of the hydroxyl group of the propargylic alcohol on the axial chlorine atom of chlorophosphite precursor **1a**: **1a$_1$** (*trans*-configuration) and **1a$_2$** (*cis*-configuration), followed by elimination of HCl. Four possibilities of intermediates were formed in pairwise equilibrium. After heating, the resulting allene **2a** was obtained with hypothetically four possibilities of conformations 2a$_1$, **2a$_1$**', **2a$_2$, 2a$_2$'**. However, only two diastereomers were detected by $^{31}P\{^1H\}$ NMR. Therefore, we turned our attention to theoretical calculation to determine the predominant conformations. In this sense, the optimized molecular structures and energies of conformations were determined using Density Functional Theory DFT/ (B3LYP 6–311++ *G* (d,p) basis set) calculations, which revealed that the **2a$_1$** conformers with the *trans* configuration and **2a$_2$** adopting a *cis* configuration are more stable by −3.05 Kcal/mol and −5.66 Kcal/mol, respectively (Fig. 3). The common point between 2a$_1$ *trans* and 2a$_2$ *cis* is that the P=O group is in the axial position. This is in agreement with our previous study [27] concerning 2-benzylamino-5-methyl-5-propyl-2-oxo-1,3,2-dioxaphosphorinane, where theoretical calculations demonstrated that conformers with the P=O group in the axial position are more stable than those with the P=O in the equatorial position. This result can be explained by a conformational stabilization due to the anomeric effect [28-29]. Moreover, the energetic stability of diastereomers **2a$_1$** and **2a$_2$** was evaluated, revealing that **2a$_1$** *Trans* is more stable by −0.14 Kcal/mol (Fig. 4).

*2.1.3. Spectroscopic characterisation and mechanistic elucidation of **3a***

Hydrazone **3a,** synthesized from the reaction between allene **2a** and hydrazine**,** was also obtained as a mixture of diastereomers, but four distinct signals were detected in the ^{31}P NMR spectrum at 21.12; 21.37; 21.55 and 21.69, respectively (Fig. 5).

To determine the optimized structures of the four detected diastereomers, mechanistic and theoretical studies were employed. Mechanistically, the hydrazine derivative reacts by nucleophilic

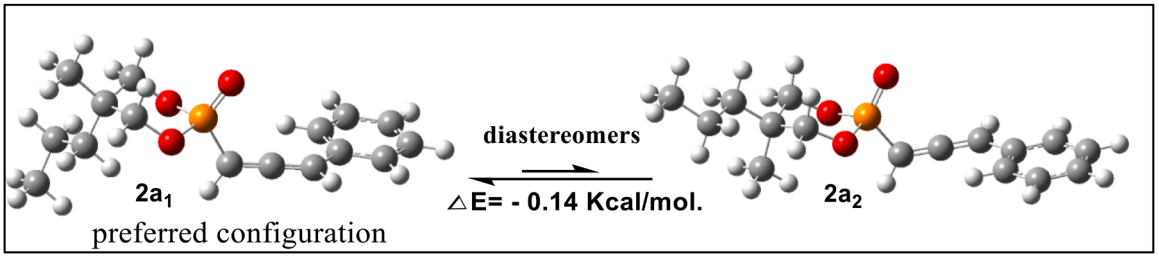

Fig. 4. Computed preferred configuration between configurations **2a$_1$ and 2a$_2$**.

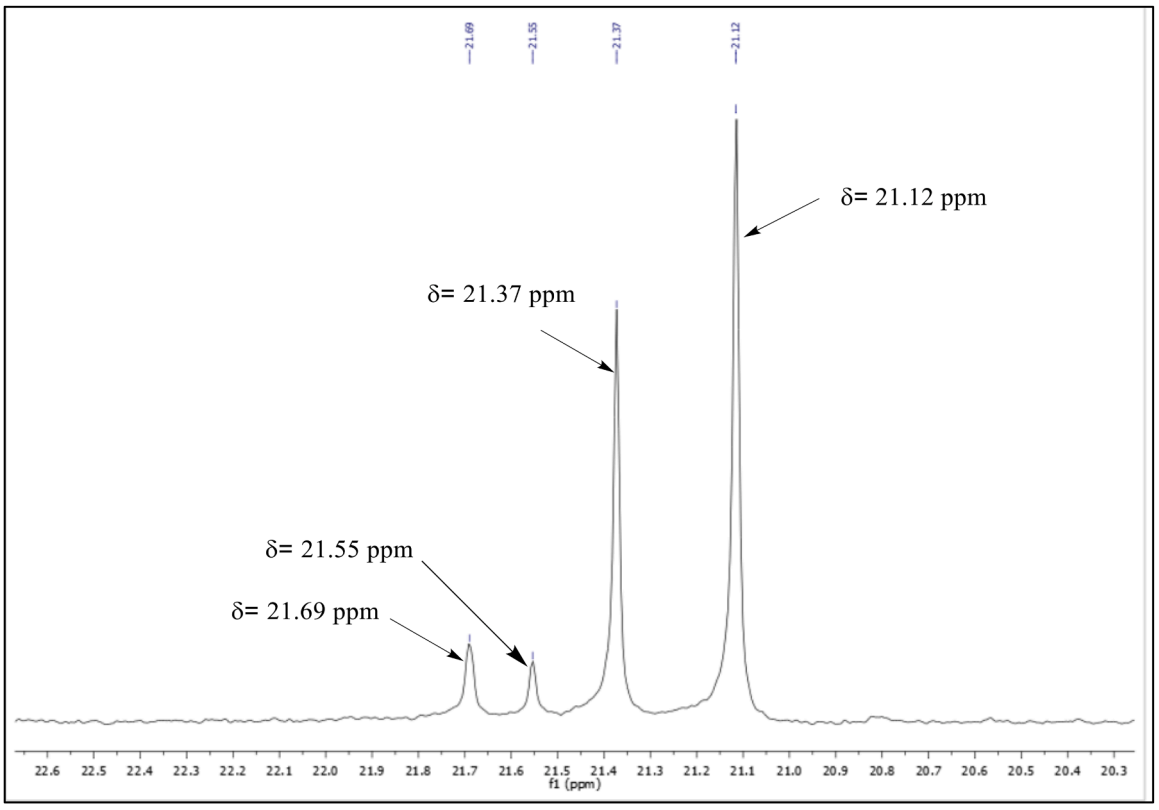

Fig. 5. $^{31}P\{^{1}H\}$ NMR spectrum of hydrazone **3a** ($CDCl_3$) revealing the presence of 4 diastereomers.

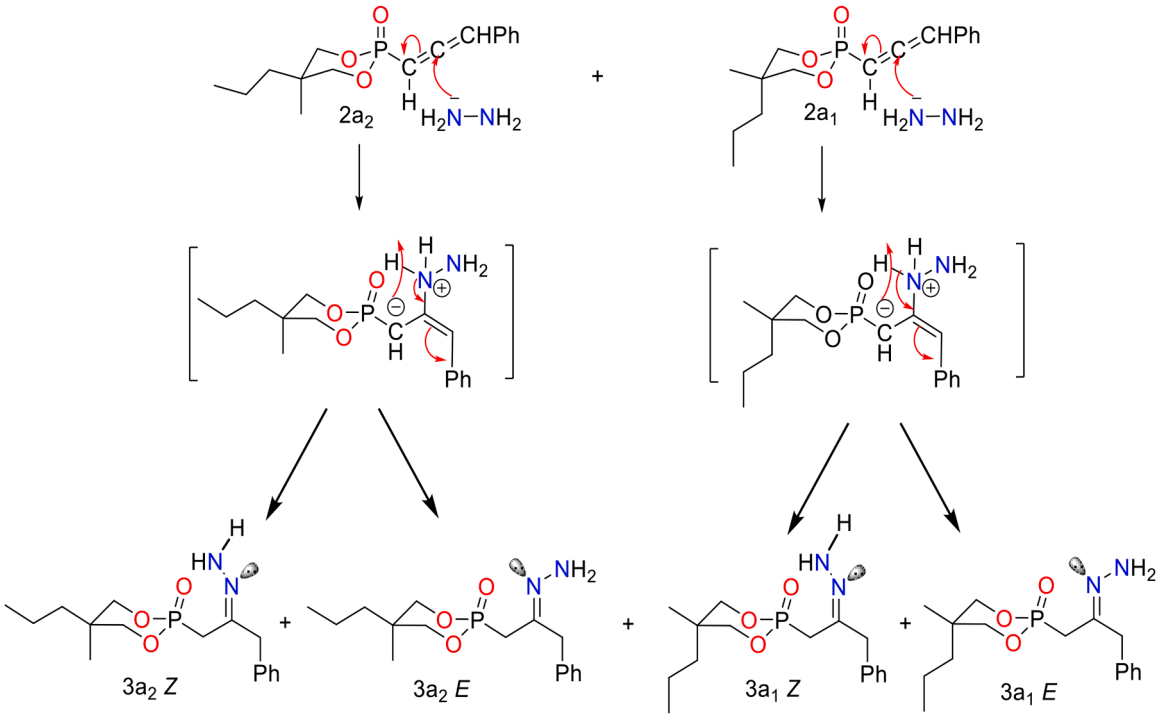

Scheme 3. Proposed mechanism for the formation of **3a**.

addition on the central allenic carbon of diastereomeric **2a (2a$_1$+2a$_2$)** to afford two enamine intermediates. Each intermediate formed undergoes rearrangement to form two isomers with different configurations: *Z* and *E* due to presence of the C=N group. In solution *Z*/*E* isomers coexist due to inversion processes at C=N bond [21,30,31]. *E*/*Z* isomerization mechanism in intramolecularly hydrogen-bonded arylhydrazones has been also assessed by DFT computing [32]. Accordingly, we obtained a mixture of four hydrazones isomers: **3a$_1$*Z*, 3a$_1$*E*, 3a$_2$*Z*, 3a$_2$*E*** (Scheme 3).

Assignment of the signals to the corresponding structure was

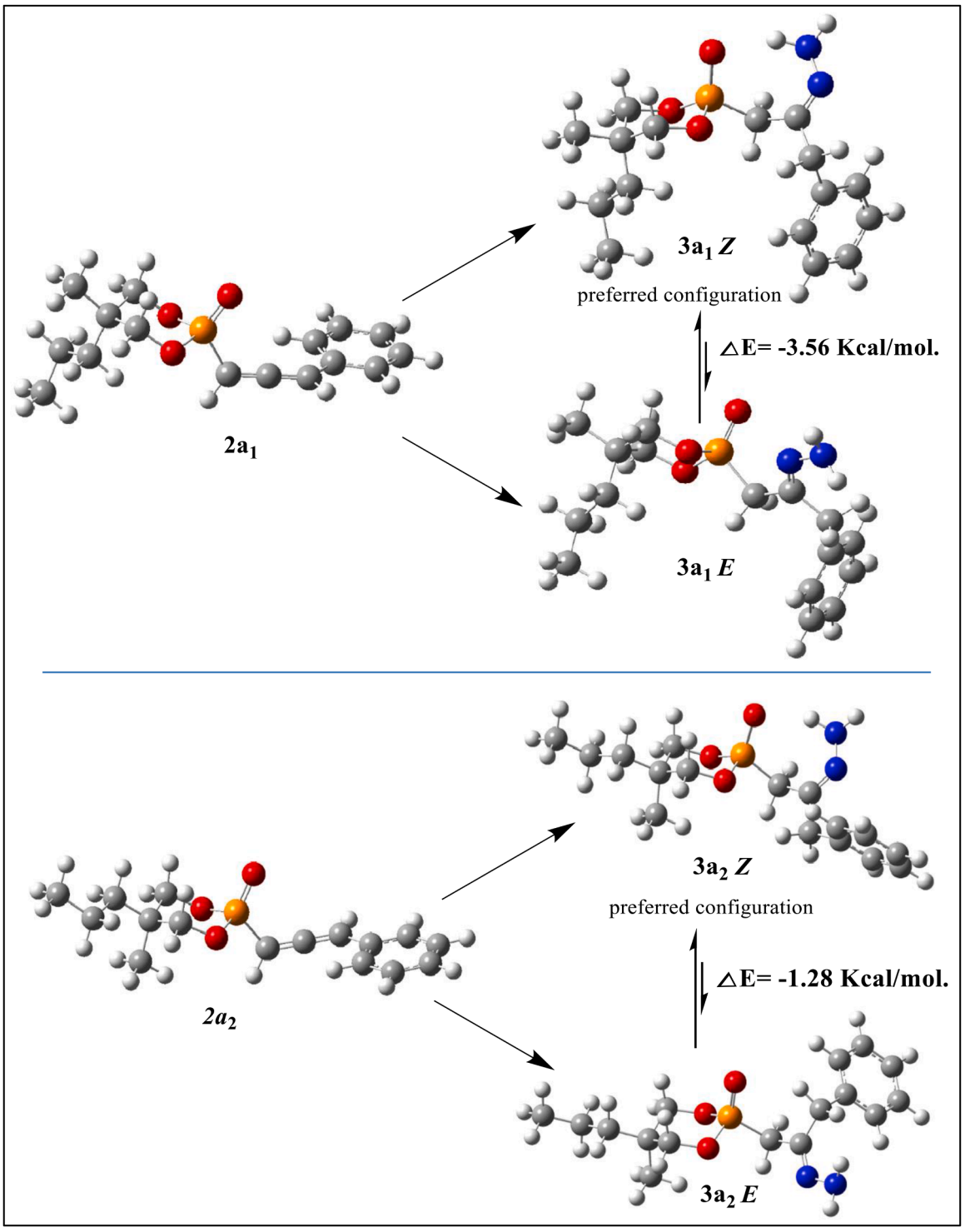

Fig. 6. Computed preferred configuration for hydrazone **3a** (**3a$_1$** ***Z*****; 3a$_1$** ***E*****; 3a$_2$** ***Z*****; 2a$_2$** ***E***).

therefore a difficult task. For this reason, our next goal was the determination of the relative stability of the four hydrazone isomers by a DFT investigation in order to assign the signals in ^{31}P NMR spectrum of **3a** and to deduce the preferred configuration. First, we studied the relative energetic stability between the couple of isomers (**3a$_1$** ***Z*** and **3a$_1$** ***E)*** formed from **2a$_1$**. It was found that **3a$_1$** ***Z*** is more stable by −3.56 Kcal/mol. Similarly, we studied the relative energetic stability of the second pair of isomers (**3a$_2$** ***Z*** and **3a$_2$** ***E***) formed from **2a$_2$**. It was found that **3a$_2$** ***Z*** is more stable by −1.28 Kcal/mol. As **2a$_1$** has the preferred configuration over **2a$_2$**, the hydrazones (**3a$_1$** ***Z*** and **3a$_1$** ***E***) obtained from **2a$_1$** predominate over the hydrazones (**3a$_2$** ***Z*** and **3a$_2$** ***E)*** obtained from **2a$_2$** (Fig. 6). Hence, the following classification of the 4 diastereomers in ascending order of energy was established as follows: **3a$_1$** ***Z*** > **3a$_1$** ***E*** > **3a$_2$** ***Z*** > **3a$_2$** ***E***. Based on this classification, signals at 21.12 ppm, 21.37 ppm, 21.55 ppm and 21.69 ppm were attributed to **3a$_1$** ***Z*** (50%), **3a$_1$** ***E*** (34%), **3a$_2$** ***E*** (7%) and **3a$_2$** ***Z*** (9 %), respectively (Fig. 7).

When analysing the reaction mixture resulting from reaction of allene **2a** with hydrazine, we observed in the ^{31}P{^{1}H} NMR an additional resonance at δ = 19.09 ppm due to another compound formed in minor amounts (Fig. S26 in Supplemental Materials). During our

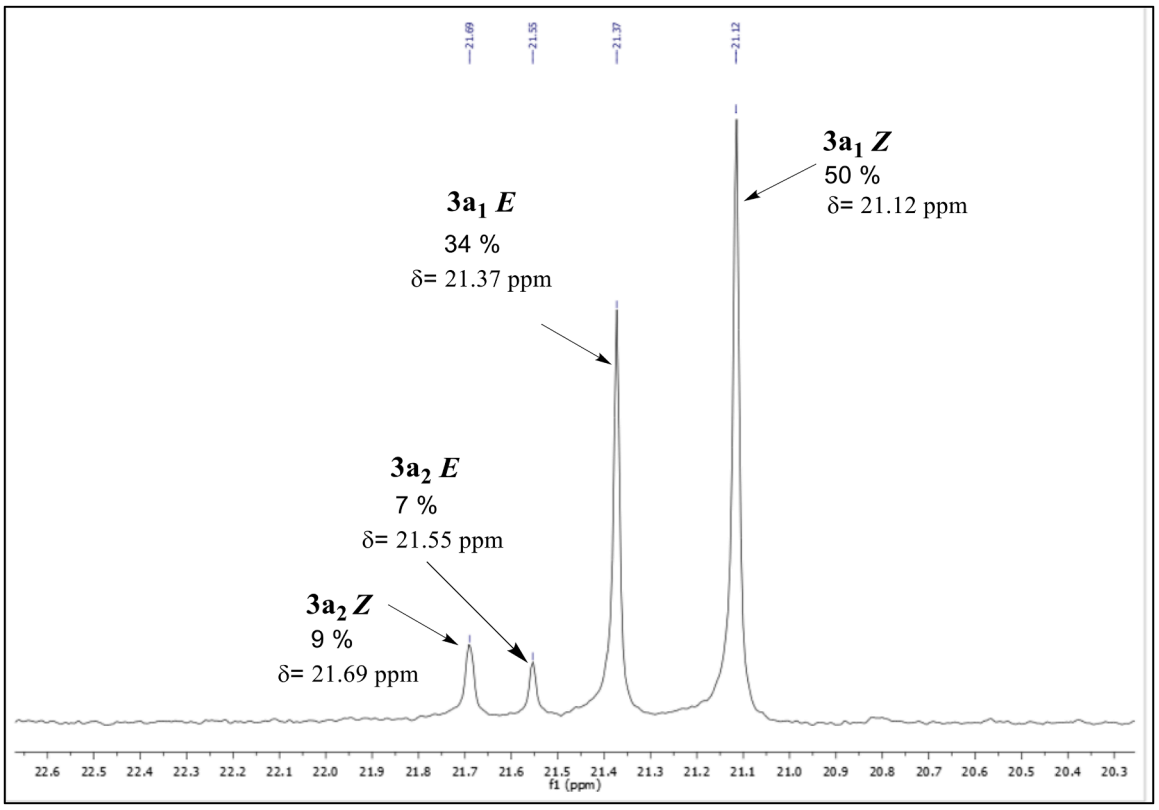

Fig. 7. Attribution of the $^{31}P\{^{1}H\}$ resonances of hydrazone **3a** to their corresponding configurations **3a$_1$*Z*; 3a$_1$ *E*; 3a$_2$ *Z*; 3a$_2$ *E***.

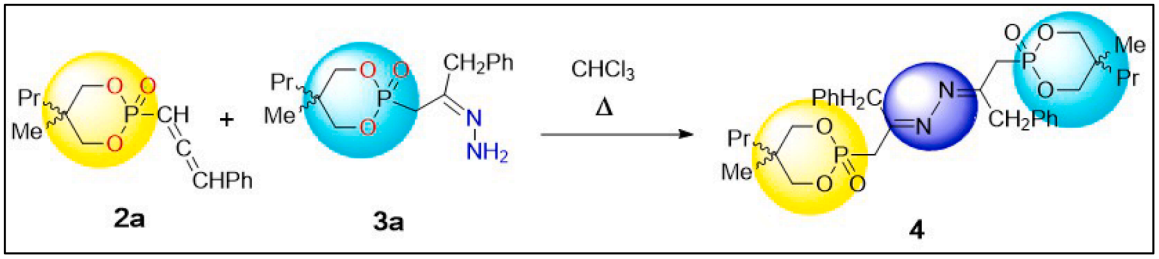

Scheme 4. Proposed mechanism accounting for the formation of azine **4** as secondary product.

attempt to obtain X-ray suitable crystals of **3a**, we failed, unfortunately, to grow crystal of **3a**. However, we noticed the formation of some colorless crystals, whose elemental analysis and crystallographic characterization (see below Fig. 9) revealed the formation of azine **4**. We suppose that formation of this symmetric azine **4** occurring in CH_3Cl solution is the result of a nucleophilic addition reaction followed by a H-shift (see Scheme 3) between the starting material, allenylphosphonate **2a** and *in situ* formed hydrazone **3a**, as outlined in (Scheme 4). Azines, with RR'C=N-N=CRR' connectivity are commonly the products of hydrazine condensation with ketone or stem from reaction of a hydrazone with a chalcone [33].

They are also used as *N,N* donor ligands in coordination chemistry [34]. So, the formation of **4** found by serendipity constitutes an alternative approach to this class of compound. Since this finding is not the topic of the present manuscript, we haven't it investigated in more detail. But this finding obtained by serendipity will be developed in future work.

*2.2. Molecular structures of 1-(2-oxo-1,3,2-dioxaphosphoranyl)−3-phenylpropanone **3c** and azine **4***

*2.2.1. Crystallographic characterisation of hydrazone **3c***

In the $^{31}P\{^{1}H\}$ NMR spectrum of compound **3c**, just a single resonance was observed, unlike for the other hydrazone products where at least two signals related to *E* and *Z* isomers are detected (Table 2). With the aim to explain this observation, a structural study of compound **3c** was carried out by single-crystal X-ray diffraction at 100 K to determine the *Z/E* configuration of **3c** and the relative orientation of the dioxaphosphorinane ring substituents. After slow evaporation of a solution of **3c** in diethyl ether, white single-crystals crystallizing in the $P2_1/c$ monoclinic space group were formed (see Table S1). Fig. 8 (top) reveals that the molecule adopts a *Z*-configuration with respect to the C=N bond, stabilized by a strong intramolecular hydrogen bond giving rise to a seven-membered ring. The connection occurs between the N-H···O=P groups (2.630 (17) Å), forming a N1-H1A···O angle of 143.6(13)°. On the other hand, the dioxaphosphorinane ring adopts a chair conformation with the P=O group in the axial position and C1 oriented in the equatorial position. A similar conformation of the dioxaphosphorinane cycle was crystallographically found for other allenylphosphonate-

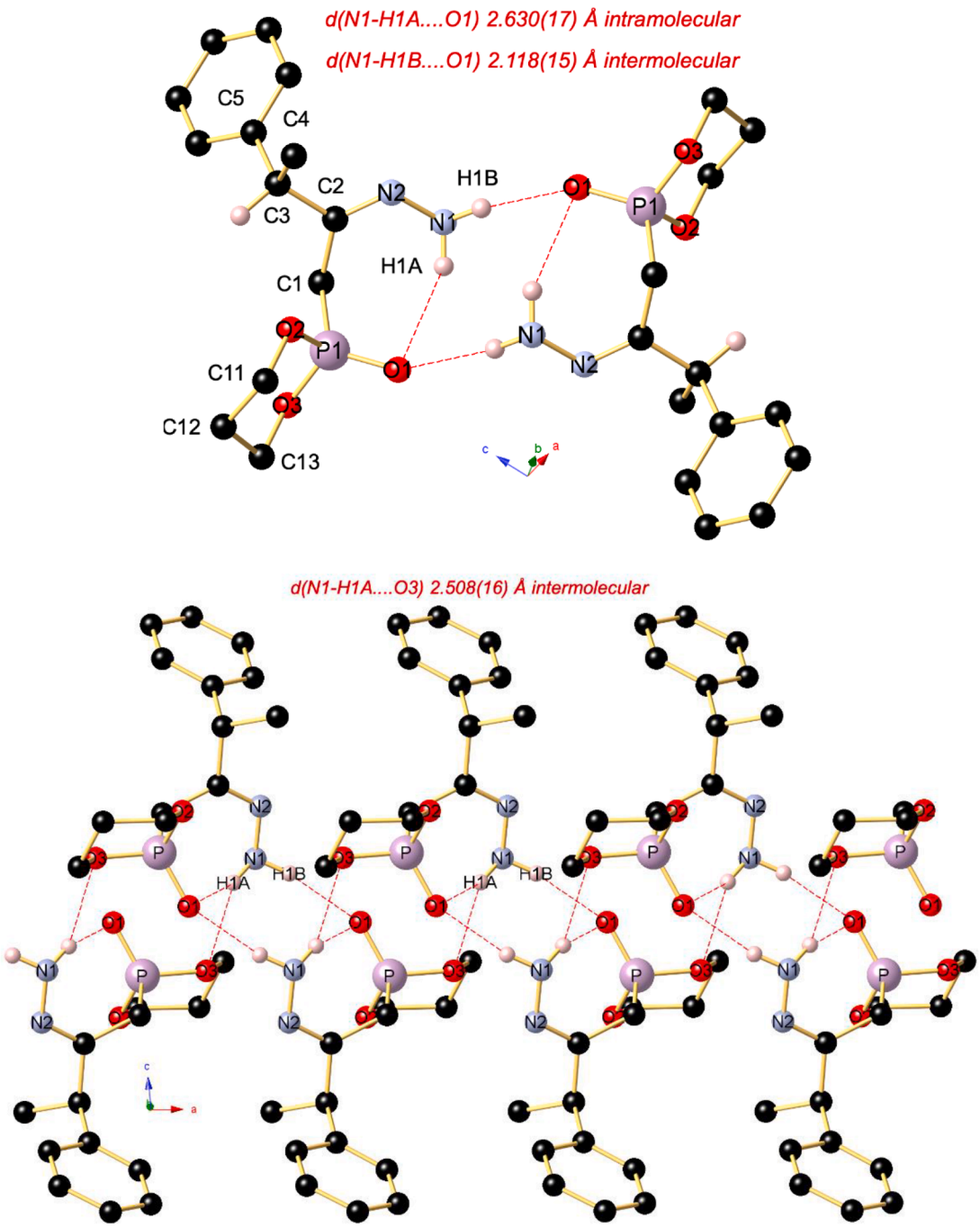

Fig. 8. (top) Molecular structure of **3c** in the crystal. Selected bond lengths (Å) and angles (°): P–O3 1.5809(6), P–O2 1.5860 (6), P–O1 1.4781(6), P–C1 1.7915 (8), O3–C13 1.4665 (10), O2–C11 1.4645 (10), N2–C2 1.2835 (10), N2–N1 1.3879(10), C2–C1 1.5165 (11), C2–C3 1.5240 (11); O3–P–O2 105.17(3), O3–P–C1 104.22 (3), O2–P–C1 103.59 (4), O1–P–O3 114.29 (4), O1–P–O2 113.84 (4), O1–P–C1 114.54 (4), P–O3–C13 117.68 (5), P–O2–C11 117.45(5), N1–N2–C2 118.35 (7). (bottom) View of a segment of the supramolecular 1D chain of **3c** generated by intermolecular N1-H1A···O3[1] hydrogen bonding. Symmetry operation to generate equivalent atoms: [1]1-*x*, 1-*y*, 1-*z*; [2]2-*x*, 1-*y*, 1-*z*; [3]–1 + *x*, −1 + *y*, +*z*.

derived organic molecules and for phosphates bearing this ring motif [35-40].

For example, the group of Sartillo-Piscil [35] demonstrated that the 2-phenoxy-2-oxo-1,3,2-dioxaphosphorinane of sugar 1,2-*O*-isopropylidene-3,5-*O*-phenoxyphosphoryl-α-*d*-glucofuranose adopts a chair conformation with the P=O group in the axial and the phenoxy group in equatorial position. This conformation is stabilized by the seven-membered intramolecular hydrogen-bonded ring structure due to the formation of O-H···O=P hydrogen bond (2.17 Å). Thus, the strong tendency of the phenoxy group to be in the axial position is diminished due to the intramolecular H-bonding. Ethyl-3-[1-(5,5-dimethyl-2-oxo-1,3,2dioxaphosphorin-2-yl)propan-2-ylidene]carbazate is another example of a hydrazone featuring an intramolecular seven-membered N-H···O=P cycle with N-H···O 2.05 Å forcing the molecule into a *cis*--chair conformation [36].

In addition to this intramolecular hydrogen bonding, an even stronger intermolecular N-H···O=P bonding of 2.118(15) Å occurs in the crystal between N1-H1···O1[2] of a neighbored molecule generating a dimeric macrocyclic motif. This hydrogen bond is further extended by a second intermolecular N1-H1A···O3[1] interaction of 2.508(16) Å

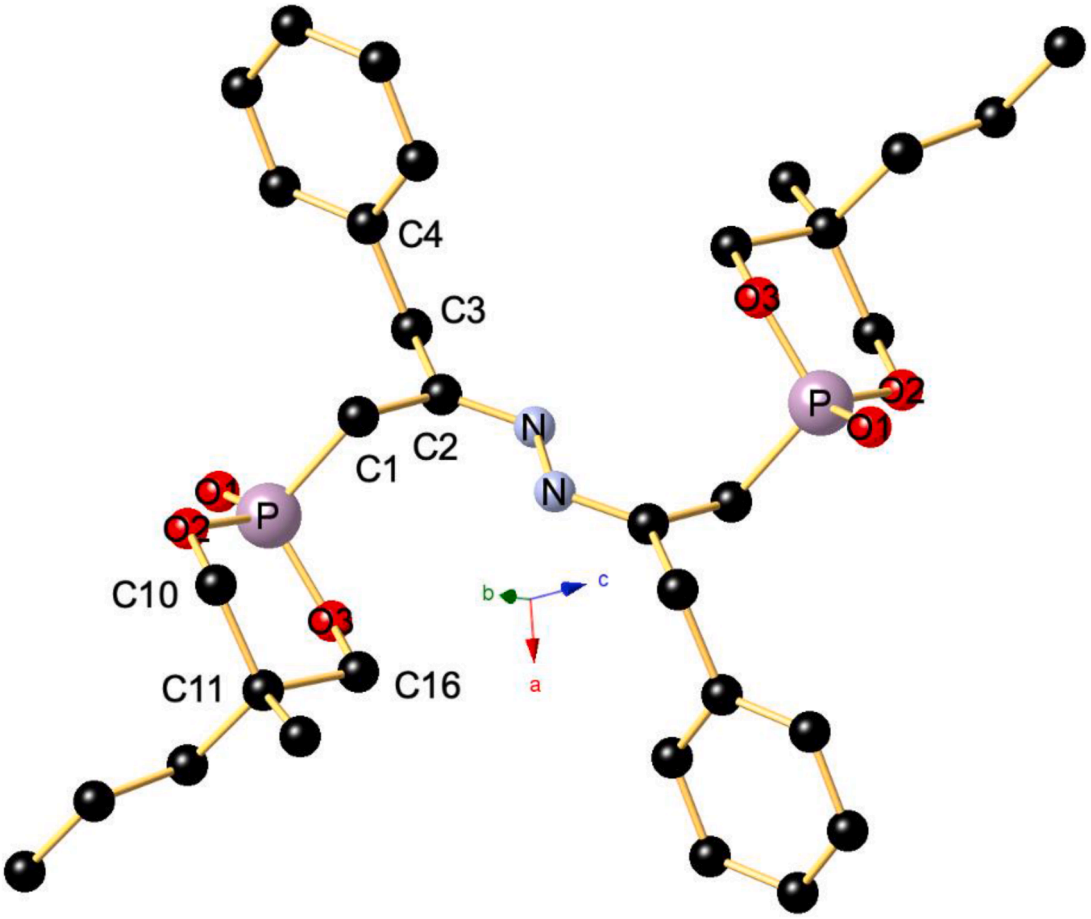

Fig. 9. Molecular structure of **4** in the crystal. Selected bond lengths (Å) and angles (°): P–O1 1.467(4), P–O3 1.585(5), P–O2 1.580(5), P–C1 1.804(4), O3–C16 1.466 (5), O2–C10 1.475(4), N–C2 1.285(4), N–N' 1.412(5); O1–P–O3 112.32(15), O1–P–O2 111.72(15), O1–P–C1 113.61(18), O3–P–C1 107.1(2), O2–P–O3 105.52(17), O2–P1–C1 106.0(2), C16–O3–P1 118.5(2), C10–O2–P 120.4(2), C2–C1–P1 112.2(2), N–C2–C1 125.3(3), N1–C2–C3 116.7(3). Symmetry operation to generate equivalent atoms: ^{1}1-*x*, 1-*y*, 1-*z*.

between the N-H function and a O3 atom of the dioxaphosphorinane cycle of an adjacent molecule, generating a supramolecular 1D ribbon (Fig. 8 bottom). A further 2D extension is secured by a short C12-H12B···N2^{3} contact of 2.584(1) Å and a C1-H1D···O1^{1} contact of 2.467 (14) Å.

Note that the occurrence of intra- and intermolecular N-H···O bonding is quite common for hydrazones having O-atoms as acceptor sites. For example, 3-ethanehydrazonoyl-4 -hydroxy-6-methyl-*2H*-pyran-2-one exhibits intermolecular N-H···O contacts of 2.221 Å along with a intramolecular hydrogen bonding between a O-H function and the sp^{2} N atom of the hydrazone (1.821 Å, CSD refcode RUZWI) [41] Another example is ethyl 7-chloro-3-(2-ethoxy-1-hydrazinylidene-2-oxoethyl)−1,1-dioxo-2, 3-dihydro-*1H*-1,2-benzothiazole-3-carboxylate displaying intramolecular — N-H···O bonding of 1.924 Å giving rise to a six-membered cycle (CSD refcode FIDDII) [42]. A third example is *N*-(2-(1-hydrazonoethyl)−3-benzofuranyl)-*p*-toluenesulfonamide forming a supramolecular 1D chain through intermolecular N-H···O=S bonding of 2.450 Å (CSD refcode TELZUF) [43].

2.2.2. *Crystallographic characterisation of azine* ***4***

The centrosymmetric molecular structure of the condensation product **4** crystallizing like **3c** in the monoclinic space group $P2_1/c$ is shown in (Fig. 9). The mid-point of the azine-type N–N bond forms an inversion center. The bond length is elongated with respect to that of **3c** (1.412(5) *vs.* 1.3879(10) Å) and matches that of other symmetric azines such as 2′-hydroxyacetophenone azine (1.415(3) Å) or (*E,E*)2,5-bis(- 5-chloro-2-methoxyphenyl)−3,4-diazahexa-2,4-diene (1.1415(5) Å). For (*E,E*)-4,4′-dimethyl-2,2′-(1,1′-dibenzylazino)diphenol bearing like **4** a benzyl substituent at the C=N carbon, a somewhat shorter N–N bond length of 1.399(3) Å) is reported [44-46].

As in the latter three examples, there is a *transoid* (or *E,E*) conformation around the C=N-N=C motif forming a torsion angle of 180° There is no intramolecular contact worth mentioning, some weaker secondary intermolecular hydrogen bonding occurs between C10-H10A···O1^{1} (2.54(4) Å), C10-H10B···O2^{2} (2.54(4) Å), and C15-H15B···O1^{1} (2.56(4) Å).

2.2.3. *Hirshfeld surface analyses of* ***3c***

To better clarify the presence of strong and weak intermolecular contacts occurring in the crystalline state, that may be complementary and relevant to the docking simulation shown in Section II.3, a Hirshfeld surface analysis was carried out utilizing the *CrystalExplorer21* software package by Spackman *et al.* [47,48]. Both intramolecular and intermolecular H-bonding was analyzed, with varying intensity and strength of these bonds. The strongest and most significant H-bond was identified as an intermolecular N1-H1B···O1 bond, which exhibits a length of 2.118 (15) Å. This bond is characterized by high linearity, indicating a significant ionic character. Apart from the very short bond length, this explains why the intermolecular interaction in the crystal is comparatively strong. In contrast, an intramolecular N1-H1A···O1 contact having a more elongated bond length of 2.630(17) Å was observed, which is weaker due to the molecular structure. Furthermore, C-H···O interactions were identified to be less pronounced on the Hirshfeld surface than the N-H···O contacts (Fig. 10). These findings indicate that in the

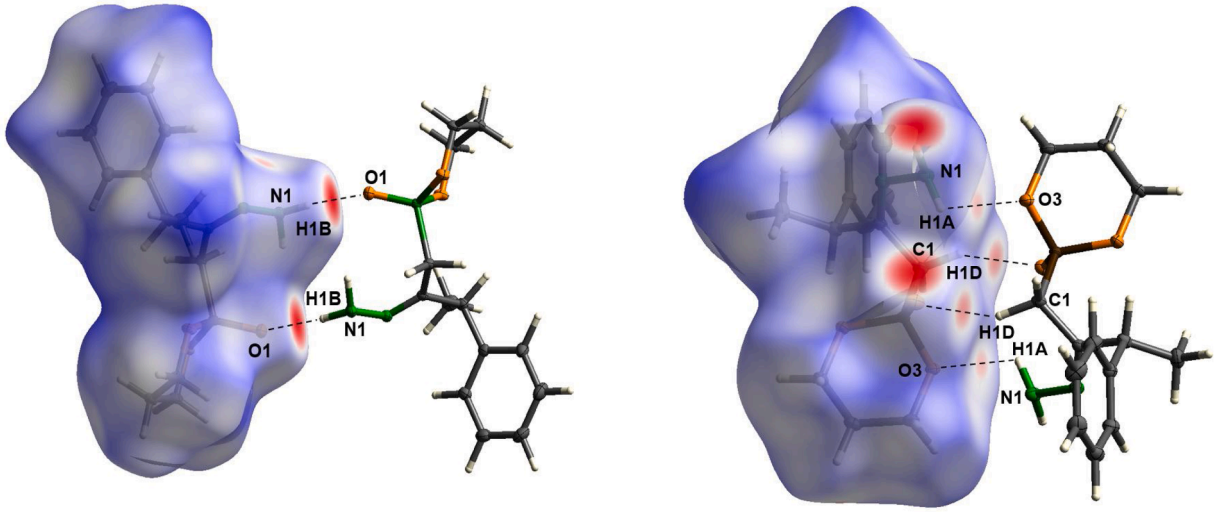

Fig. 10. Hirshfeld-surface of **3c**, indicating a strong intermolecular bonding between two **3c** molecules in the elementary cell with d_{norm} –0.4503 to 1.4815 a.u (left); some weaker intermolecular interactions occurring in **3c** on the same Hirshfeld surface with d_{norm} –0.4503 to 1.4815 a.u. (right).

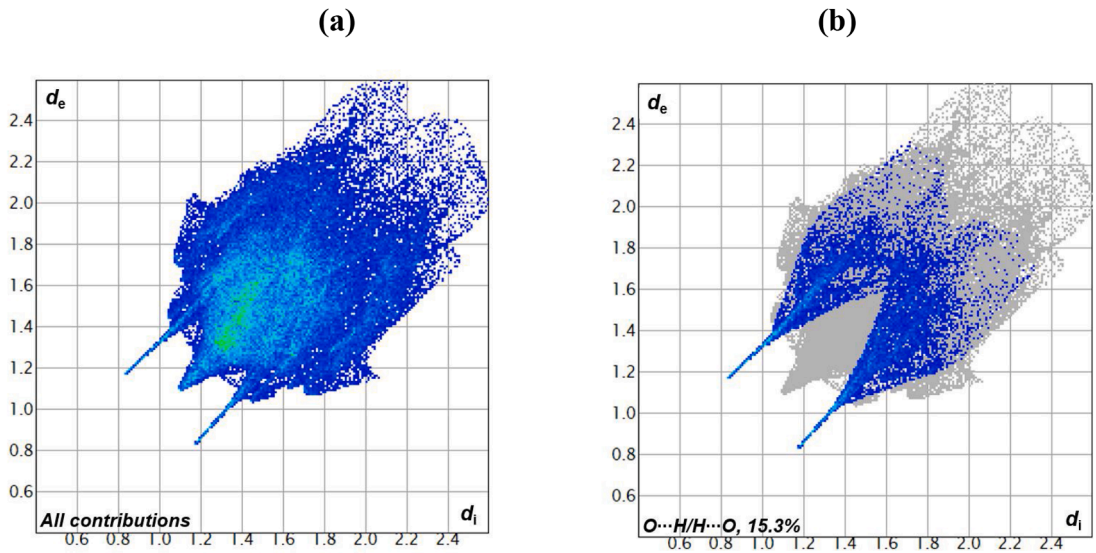

Fig. 11. 2D-fingerprint plots of **3c** showing all contributions (a) and resolved into O···H/H···O- percentages participations (b).

present molecule, especially the N-H···O contacts are crucial for supramolecular interactions with other molecules.

Fig. 11 depicts the 2D-fingerprint plots showing all contribution plot and O···H/H···O- contacts. The plots depicting the percentages participations to the total Hirshfeld surface area due to N···H/H···N-, C···H/H···N- and H···H-contacts are presented in the Supporting Material as Fig. S45.

*2.2.4. Theoretical study of the Z/E **3c** isomer stability and comparison of theoretical and experimental geometric properties of **3c** Z*

To study the relative stability of the *Z/E* configuration of **3c** in the gas and solvent (chloroform) phases, a DFT calculation was performed using the B3LYP/ 6–311++ *G* (d,p) basis set. The optimized molecular geometries of **3c** both with *Z* and *E* configuration are shown in Fig. 12. These calculations in both gas and solvent phases confirm that the *Z*-isomer is more stable than the *E*-isomer. In fact, **3c** *Z* is more stable by −11.82 Kcal/mol and by −9.11 Kcal/mol in gas-phase and solvent phase, respectively. This result agrees with the crystal structure revealing a *Z*-configuration with a strong intramolecular H-bond (Fig. 8). Accordingly, the singlet observed in the ^{31}P NMR spectrum at 20.8 ppm is attributed to **3c** with *Z* configuration (Table 2). A comparison of the theoretical optimized structure of **3c *Z*** investigated by DFT in the gas-phase, in $CHCl_3$ and the experimental structure obtained by SCXRD was conducted. The selected geometrical parameters are as follows: the bond length and angles values of **3c** *Z* isomer found by DFT (in the gas-phase and in $CHCl_3$) and by SCXRD are outlined in Table 3. It can be deduced that they match well with correlation coefficients of R^2 = 0.9892, R^2 = 0.9930 for bond length (DFT (gas)/ SCXRD), (DFT ($CHCl_3$)/ SCXRD), respectively and R^2 = 0.9514 and R^2 = 0.9147 for angles (DFT (gas)/ SCXRD) and (DFT($CHCl_3$) / SCXRD), as displayed in Fig. 13.

Table 4 lists the O···H distance (SCXRD/DFT) and angle θ (O···H-N) (SCXRD/DFT) in hydrazone **3c *Z***. The distances between O and H calculated by DFT/B3LYP are 2.094 Å and 2.115 Å for the gas-phase and chloroform, respectively. These values match with those reported in the literature [49,50]. The angles (O···H-N) calculated by DFT/B3LYP in both phases are around 154° These values are among 90–180° that is determined for hydrogen-bond. These results reflect that there is an intramolecular hydrogen bond between oxygen and hydrogen in the optimized structure of **3c *Z*** (Fig. 12). The geometrical properties of **3c *Z***

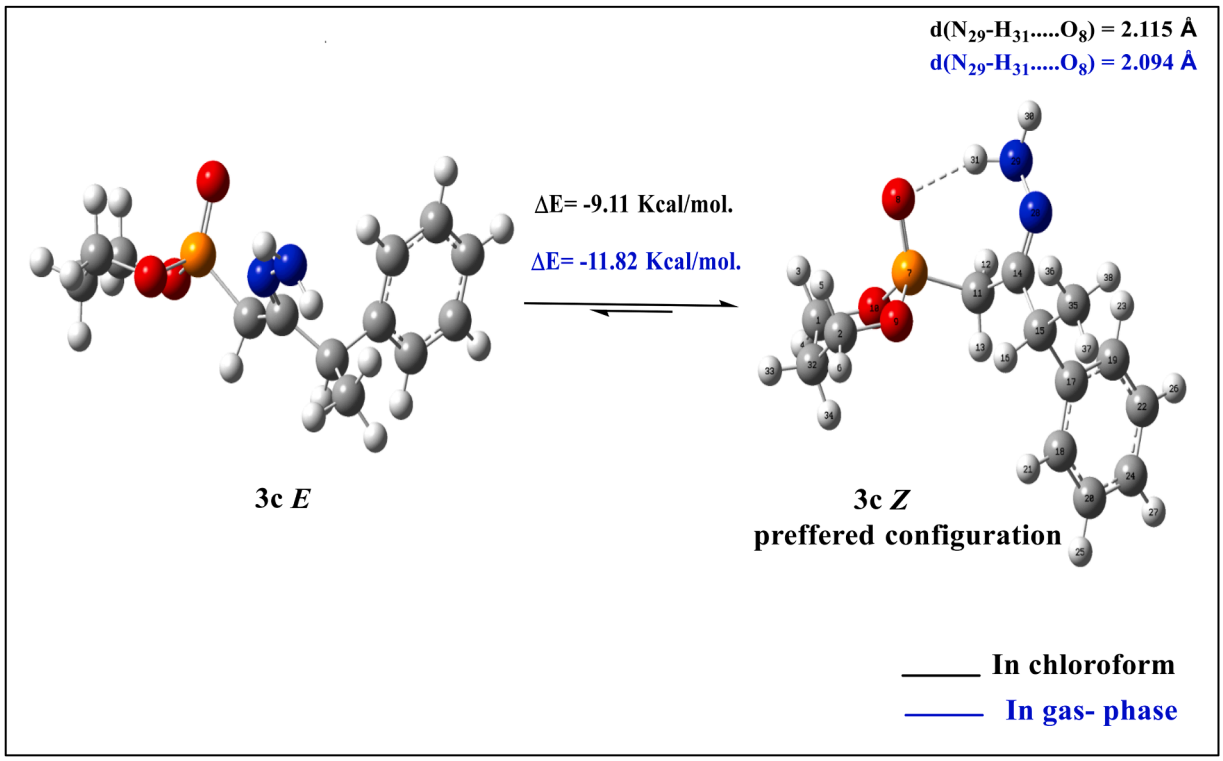

Fig. 12. Optimized geometries for the ***Z/E*** isomers of hydrazone **3c**.

Table 3
Selected bond lengths (Å) and angles (°) from X-ray diffraction and DFT optimization for **3c *Z*** isomer.

Bond lengths (Å)	Exp SCXRD	Calc. in gas	Calc. in $CHCl_3$	Angles (°)	Exp SCXRD	Calc. in gas	Calc. in $CHCl_3$
P7=O8	1.478(6)	1.488	1.493	C14=N28-N29	118.35(7)	119.01	118.98
P7-C11	1.7915(8)	1.805	1.808	P7-C11-C14	111.12(5)	113.82	114.05
P7-O10	1.5809(6)	1.626	1.619	C11-C14=N28	124.77(7)	123.93	124.03
P7-O9	1.5860(6)	1.626	1.619	O8=P7-C11	114.54(4)	115.16	114.30
C14=N28	1.283(10)	1.278	1.278	O8=P7-O9	113.84(4)	114.76	114.78
N28-N29	1.387(10)	1.384	1.388	O8=P7-O10	114.29(4)	114.59	114.60
C11-C14	1.5165(11)	1.522	1.520	C11-C14-C15	117.14(7)	116.61	116.43
C14-C15	1.5240(11)	1.522	1.522	N28=C14-C15	118.04(7)	119.35	119.44
C15-C35	1.5267(13)	1.536	1.536	C14-C15-C35	111.61(7)	113.20	113.49

*The atom numbering is shown in the optimized ***Z*** configuration of **3c**.

alter slightly in the gas-phase or in the presence of chloroform as solvent. On the other hand, a comparison of the calculated and experimental SCXRD geometrical properties shows that they are quite similar.

2.2.5. *Theoretical/ experimental infrared characterisation of **3c***

The experimental IR spectral data of **3c (**black in Fig. 14, see also Fig. S49) show characteristic absorption bands in the range of 2900–3500, 1600–1700, 1250–1300 and 1000–1200 cm^{-1} which may be assigned to ν(NH), ν(C=N), ν(P=O) and ν(P-O-C), respectively. This is consistent with the literature data [51-55] and also with the computed wave-numbers used to plot the theoretical spectrum **(**red in Fig. 14, see also Fig. S51). The theoretical spectrum was determined after optimization of the **3c** structure using Gaussian 09 with B3LYP/ 6–311++ *G* (d.p) basis set. In the experimental spectrum, the N-H bond gives rise to broad band between 2900 and 3500 cm^{-1} indicating that the N-H groups are engaged in intramolecular and intermolecular hydrogen bonding, in line with the crystal structure (Fig. 8.). This broadness is in accordance with the IR features described in related work dealing on compounds exhibiting a H-N···O hydrogen bonding [56-58].

2.3. *Molecular docking of the β-cycloalkoxyphosphonated hydrazones*

The current work investigated by molecular docking the interactions of β-cycloalkoxyphosphonated hydrazones **3a-f** as hosts with the active binding site of both enzymes Butyrilcholinesterase (BuChE) (PDB ID: 4BDS) and Acetylcholinesterase (AChE) (PDB ID: 4EY7). Tacrine

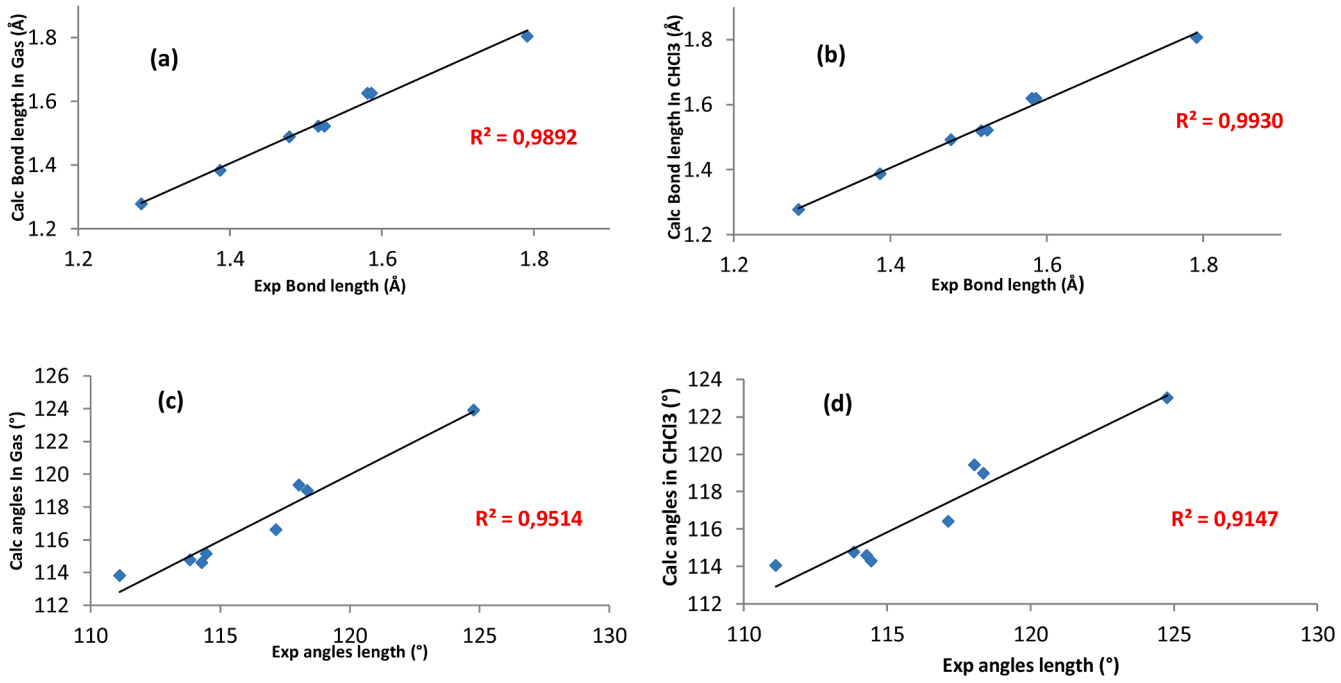

Fig. 13. DFT/SCXRD graphical correlation for bond lengths of **3c** ***Z*** (**a:** calculated bond lengths in the gas-phase **b**: calculated bond lengths in $CHCl_3$) and bond angles (**c**: calculated angles gas-phase **d**: calculated angles in $CHCl_3$).

Table 4
Comparison of **3c** ***Z*** isomer H-bond distance (Å) and angle (°) from X-ray diffraction and DFT optimization.

		d (O···**H-N**) (Å)	θ (O···**H-N**) (°)
DFT (3c *Z*)	gas-phase	2.094	154.44
	in $CHCl_3$	2.115	154.14
SCXRD (3c *Z*)		2.630 (17)	143.60(13)

(https://en.wikipedia.org/wiki/Tacrine) and Donepezil (https://en.wikipedia.org/wiki/Donepezil), two acetylcholinesterase inhibitors employed for the treatment of Alzheimer disease [59-62], were used as reference standards in our study. One of the common features occurring in these reference molecules and hydrazones **3** is that they contain nitrogen atoms in their scaffolds. They also incorporate heterocyclic rings and six-membered aromatic cycles capable of interacting with the active site (Fig. 15). In the literature, there are compounds with some or all of these features that have shown confirmed inhibitory activity for one or both proteins [14-16,63-65]. For example, tert-butyl -*N*-(3-(2, 3-dimethoxyphenyl)−2-phenylpropyl)sulfamoylcarbamate with a phenyl group and a N-atom in its backbone shows a high inhibitory effect against AChE [64]. Further examples [14-16] are given in Fig. 1.

Hence, we decided to employ *in silico* molecular docking simulations to test our synthesized hydrazones. To assess whether hydrazones **3** could represent potential candidates for inhibition of both proteins, an investigation based on free energies released as the ligands bind to the proteins as well as their binding mechanism to key residues, has been conducted.

2.3.1. *Active sites of AChE and BuChE*

According to previous studies [66-68], it is confirmed that the structure of AChE possesses a catalytic active site (CAS), a 20 Å-deep gorge and a peripheral anionic site (PAS). The active site residues of the catalytic triad are: SER203, HIS447, GLU 334. This active site has a subside involving TRP86. The PAS of AChE contains TYR72, ASP74, TYR124, TRP286, SER293 and TYR341. The overall structure of BuChE is similar to that of AChE with 65 % of the amino acids in common. The difference lies in the acyl-binding pocket which is larger in BuChE than in AChE. The catalytic triads of BuChE consist of the following amino acids: HIS438, SER198, GLU325. There are key residues: TYR332, PHE329, TRP82 belonging to the anionic site, which is essential for the reaction. In addition, the oxyanion hole, incorporating GLY116, GLY117 and ALA119, stabilizes the transition-state through hydrogen-bond interactions [69,70]. These amino acids are important for the active site of both AChE and BuChE.

2.3.2. *Interactions of references and compounds with BuChE and AChE receptors*

The interactions of Tacrine with BuChE as well as that of Donepezil

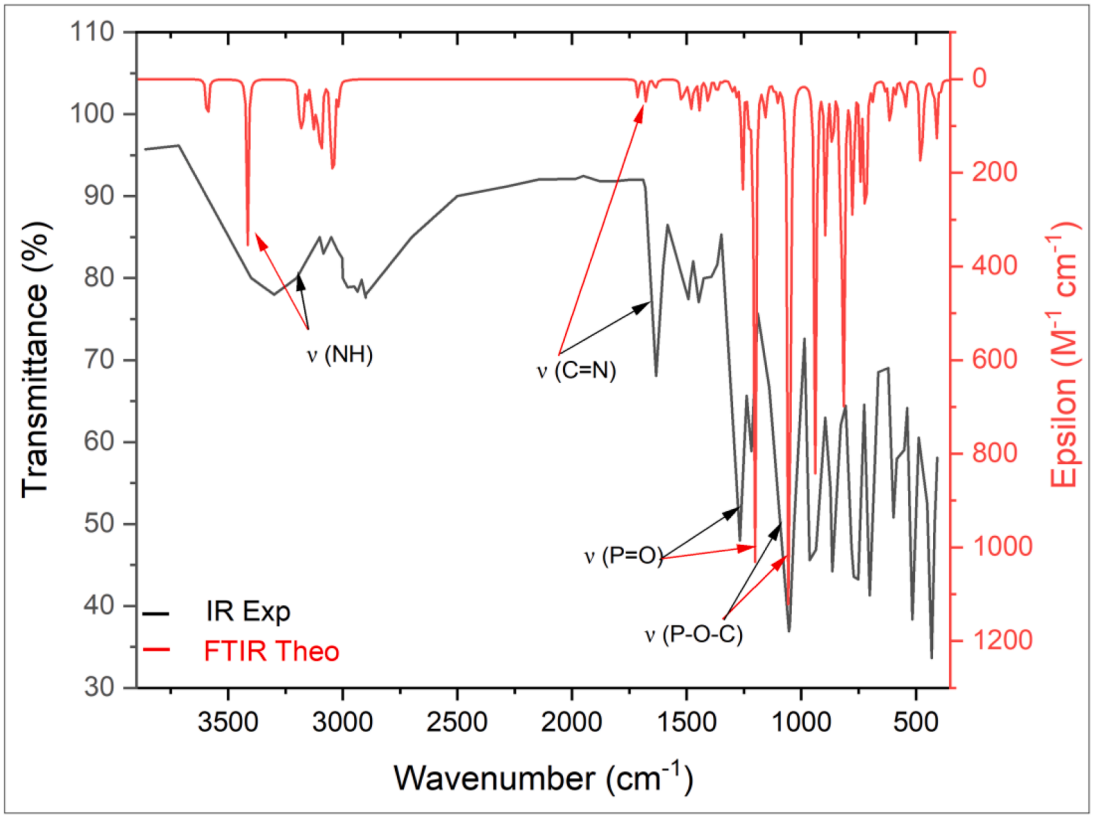

Fig. 14. Theoretical (red) and experimental (black) ATR-IR spectra of **3c**.

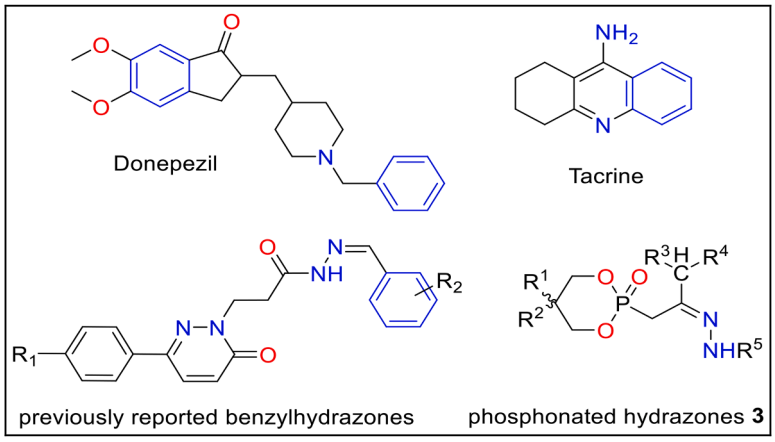

Fig. 15. Structures of reference molecules (Donepezil and Tacrine), and previously reported benzylhydrazones [14] and our phosphonated hydrazones **3**.

with AChE were analysed to predict their binding mode using the AutoDock vina Software [71]. Results are reported in Table 5 and 6. All compounds were docked into the same groove of the native co-crystallized binding site of both proteins.

Firstly, we studied the interaction between the hydrazone derivatives and BuChE. It is important to note that all **3a-f** compounds exhibit different types of interaction (H-bond, Van der Waals…) with key residues of the BuChE active site. All six **3a-f** hydrazones subjected

Table 5
Interactions occurring between the ligand and BuChE: binding affinity, number of conventional hydrogen bonds and interacting amino acid residues.

Ligand	Estimated free energy of binding (kcal/mol)	Intermolecular interactions			
		Interacting amino acid residues	Conventional hydrogen bonds		
			Number of H-bonds	Involved amino acid Residue	Distance (Å)
3a	−7.8	TRP82, GLY116*, GLY117, GLN119, THR120**, SER198, TRP231, PRO285, LEU286, VAL288, ALA328, PHE329, PHE398, HIS438, GLY439,	3	GLY116 THR120	1.71 2.85 2.89
3b	−5.5	TRP82, GLY115, GLY116, THR120, TYR128, GLU197*, SER198, ALA199, ALA328, PHE32 9, TRP430, MET437, HIS438*, GLY439, TYR440	2	GLU197 HIS438	2.53 2.09
3c	−7.1	TRP82, GLY116*, GLY117, THR120*, SER198, TRP231, LEU286, VAL288, PHE329, ALA328, TYR332, PHE398, HIS438	2	GLY116 THR120	2.93 2.36
3d	−7.4	ILE69, ASP70, SER79, TRP82, ASN83, GLY116*, GLY117, GLN119, THR120**, SER198, TRP231, PRO285, LEU286, VAL288, PHE329, PHE 398	3	GLY116 THR120	1.85 3.03 2.88
3e	−7.7	TRP82, GLY116*, GLY117, GLN119, THR120*, SER198, TRP231, PRO285, LEU286, VAL288, ALA328, PHE329, TYR332, PHE 398, HIS438,	2	GLY116 THR120	2.20 2.49
3f	−7.5	ASP70, SER79, TRP82, GLY116, GLY117, SER198, TRP231, PRO285*, LEU286, VAL288, PHE329, PHE398, HIS438	1	PRO285	2.58
Tacrine[R1]	−8.1	TRP82, GLY115, GLY116, GLU197, SER198, ALA328, TYR332, TRP430, MET437, HIS438, GLY439, TYR440	0	-	-

R1: Reference 1; *: Amino acid residue involved in H-bond formation.

Table 6
Interactions occurring between the ligand and AChE: binding affinity, number of conventional hydrogen bonds and interacting amino acid residues.

Ligand	Estimated free energy of binding (kcal/mol)	Intermolecular interactions			
		Interacting amino acid residues	Conventional hydrogen bonds		
			Number of H-bonds	Involved amino acid Residue	Distance (Å)
3a	−7.2	TYR72, TYR124, TRP286, LEU289, GLN291, GLU292, SER293*, VAL294, PHE295, ARG296*, TYR341	2	SER293 ARG296	2.56 2.80
3b	−6.4	ASP74*, THR83, TRP86, GLY121, GLY122, TYR124**, SER125, SER203, PHE297, TYR337, PHE338, TYR341*, HIS447	4	ASP74 TYR124 TYR341	2.10 3.12 3.12 2.36
3c	−8.9	TRP86, GLY121, GLY122, TYR124*, SER125, TRP286, VAL294, PHE295, PHE297, TYR337, PHE338, TYR341, HIS447	1	TYR124	3.25
3d	−9.2	ASP74*, THR83, TRP86, GLY121, TYR124*, TRP286, VAL294, PHE295, PHE297, TYR337, PHE338, TYR341*, HIS447	3	ASP74 TYR124 TYR341	1.99 3.03 2.31
3e	−7.0	TYR124, TRP286, LEU289, GLN291, GLU292, SER293*, VAL294, PHE295, ARG296*, PHE297, PHE338, TYR341	2	SER293 ARG296	2.51 2.59
3f	−9.4	ASP74*, THR83, TRP86, GLY120, GLY121, TYR124*, GLU202, TRP286, VAL294, PHE295, PHE297, TYR337, PHE338, TYR341*, HIS447, GLY448	3	ASP74 TYR124 TYR341	2.28 3.07 2.10
Donepezil[R2]	−11.6	TYR72, ASP74, TRP86, GLY121, TYR124, GLU202, TRP286, LEU289, VAL294, PHE295*, ARG296, PHE297, TYR337, PHE338, TYR341, HIS447, GLY448	1	PHE295	3.05

R2: Reference; *: Amino acid residue involved in H-bond formation.

to molecular docking display H-bonding whereas the reference drug does not present any H-bonding. According to the literature [72], a hydrogen bond with a bond distance < 3.1 Å is considered as a strong one. Thus, compounds **3a** and **3d** showed the highest number of conventional H-bonds (3 strong H-bonds). In fact, compound **3a** is bonded to the oxyanion hole amino acid GLY116 by one strong hydrogen bond (bond distance = 1.71 Å) and to another THR120 residue with two strong hydrogen bonds (bond distances = 2.85 Å; 2.89 Å). Similarly, compound **3d** establishes a strong hydrogen bond with GLY116 (bond distance = 1.85 Å) and two strong H-bond with THR120 (bond distances = 2.88 Å; 3.03 Å). In addition to hydrogen bonding, compounds **3a-f** exhibit other types of interaction with important residues of the active site. In fact, compound **3a** interacts with residues of the catalytic triad as follows: Van der Waals interaction with amino acids SER198 and HIS438. Also, we note interactions with the anionic site: a π-sigma interaction with amino acid TRP82 and a T-shaped π-π interaction with PHE329. Compound **3d** exhibits a Van der Waals contact with the SER198 residue of the catalytic triad, a π-alkyl interaction and a T-shaped π-π interaction with the anionic site residues PHE329 and TRP82, respectively. These described interactions indicate that compounds **3a** and **3d** can be stable within the BuChE active site. With regard to the binding energy score, Tacrine showed a lower binding energy score −8.1 kcal/mol compared to the six hydrazone derivatives (−7.1 kcal/mol to −7.8 kcal/mol). **3a** owns the best binding energy score (−7.8 kcal/mol), followed by compound **3e** (−7.7 kcal/mol) and **3d** (−7.4 kcal/mol), reflecting high affinity with the active site.

Based on these findings, it appeared promising for forthcoming studies to assess the *in vitro* inhibitory activity of **3a** and **3d** against BuChE. Table 5 summarizes the docking results for BuChE: binding energy score, conventional H-bonds, distances and interacting amino

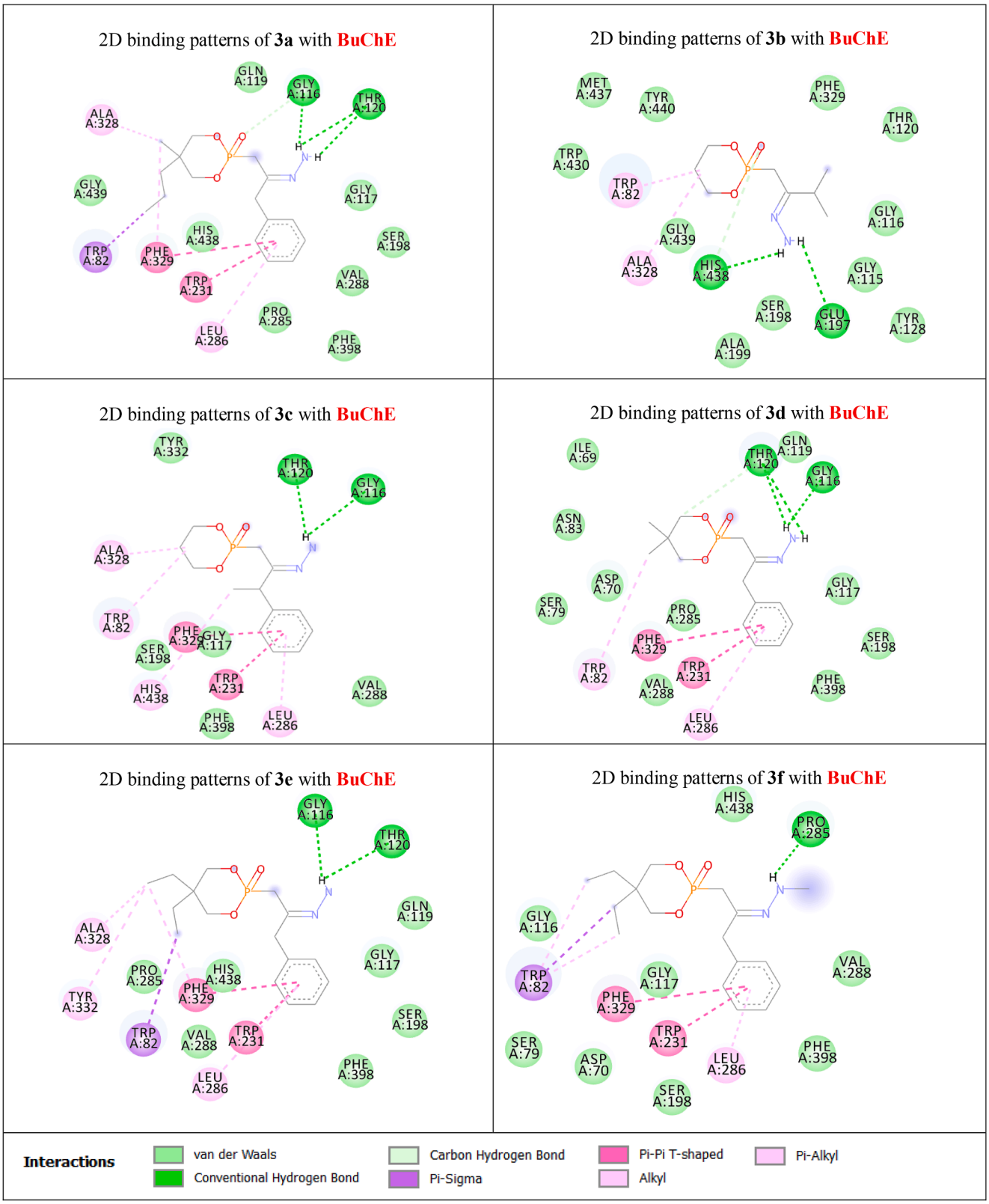

Fig. 16. 2D binding patterns of hydrazone derivatives **3a-f** with **BuChE** (PDB: 4BDS).

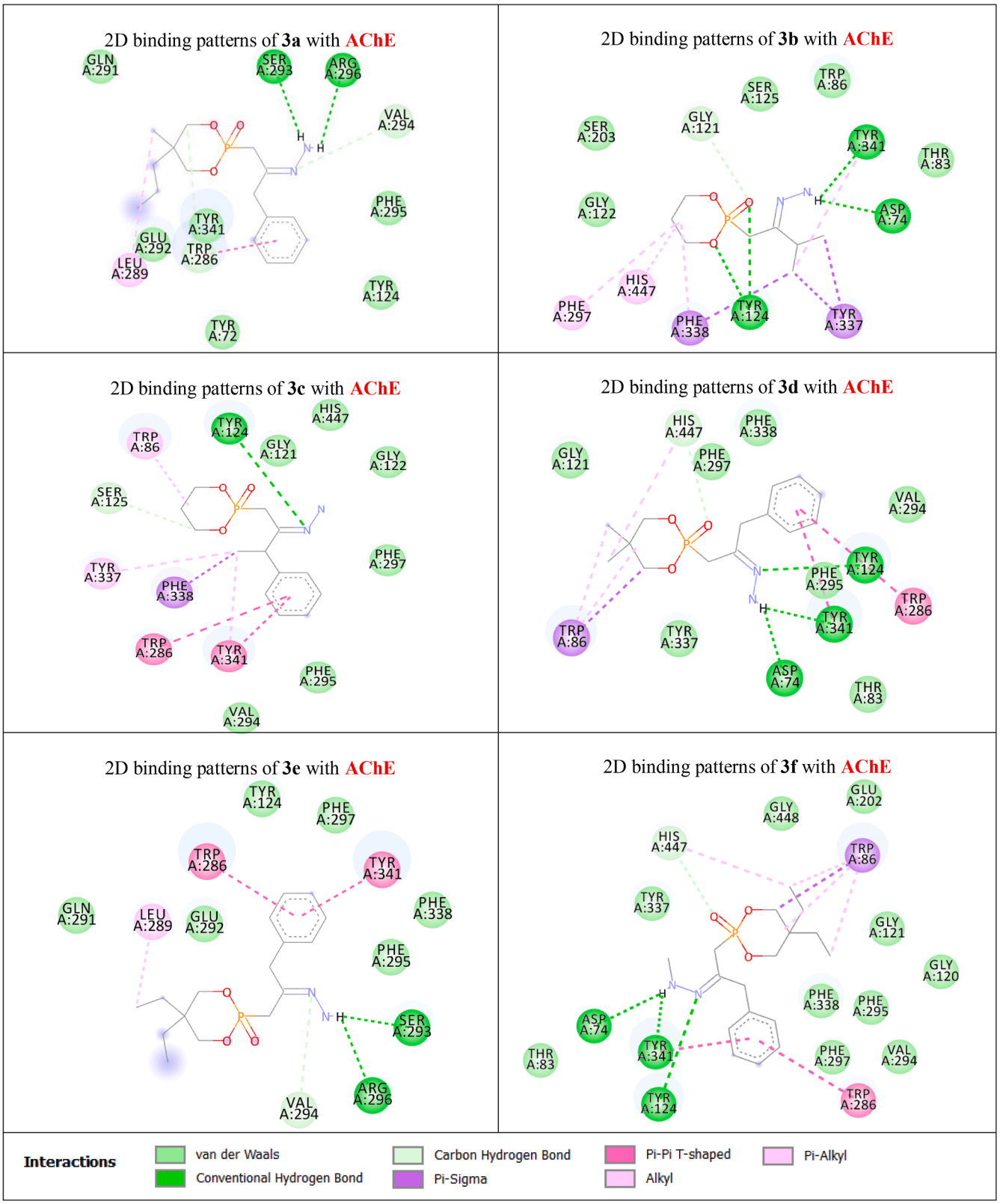

Fig. 17. 2D binding patterns of hydrazone derivatives **3a-f** with **AChE** (PDB: 4EY7).

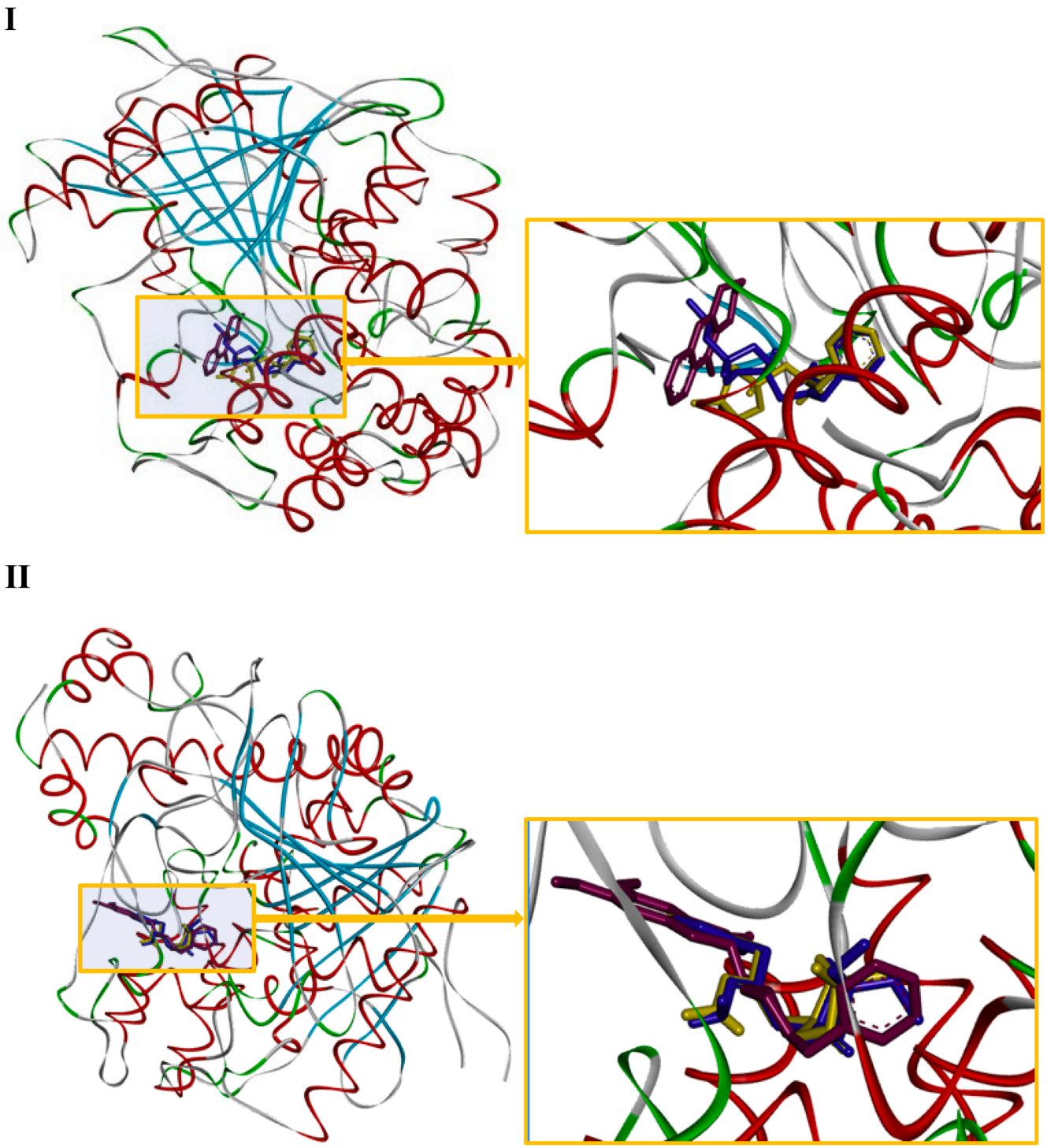

Fig. 18. Presentation of the best docking conformations of compounds **3** and references into BuChE and AChE active sites. **I**: Compound **3a** (blue), **3d** (yellow) and **Tacrine** (purple) are inserted into **BuChE** (PDB ID: 4BDS); **II**: Compound **3f** (blue), **3d** (yellow) and **Donepezil** (purple) are inserted into **AChE** (PDB ID: 4EY7).

acid residues.

Fig. 16

Then, we proceeded to study the interaction between hydrazones **3a-f** and AChE (Fig. 17). We found that most of tested compounds form more than one H-bonds with certain key amino acid residues in the active site compared to Donepezil, which present only one H-bond with the amino acid PHE295 (bond distance = 3.05 Å). However, Donepezil has a better binding energy score of −11.6 kcal/mol compared to compounds **3a-f** (−6.4 kcal/mol to −9.4 kcal/mol) (Table 6). The **3d** derivative has a binding energy score of −9.2 kcal/mol and generates 3 strong H-bonds with amino acids of the PAS pocket as follows: ASP74 (bond distance = 1.99 Å), TYR124 (bond distance = 3.03 Å), TYR341 (bond distance = 2.31 Å). On the other hand, compound **3f** exhibits −9.4 kcal/mol as binding energy score and establishes 3 strong H-bonds with PAS pocket residues: ASP 74 (bond distance = 2.28 Å), TYR124 (bond distance = 3.07 Å), TYR341 (bond distance = 2.10 Å). Additionally, both **3d** and **3f** interact via a Carbon-Hydrogen contact with HIS447 residue of the catalytic triad and make a π-sigma contact with a key amino acid: TRP86.

Because of their high binding energy values and several interactions

Table 7
ADMET and drug-likeness properties of compounds **3a, 3d** and **3f**.

Entry	MW[a] (g/mol)	TPSA[b] (Å^2)	n-ROTB[c]	MLog P[d] WLog P[d`]	*n*- H bond acceptors[e]	*n*- H bond donors[f]	Lipinski's violation	Verber violation	Egan violations	PAINS[g] alert
	<500	<140	<11	≤ 5	<10	<5	≤1	≤1	≤1	
3a	324.36	83.72	6	2.08 3.59	5	1	Accepted	Accepted	Accepted	0 alert
3d	296.30	83.72	4	1.57 2.81	5	1	Accepted	Accepted	Accepted	0 alert
3f	338.38	69.73	7	2.32 3.85	5	1	Accepted	Accepted	Accepted	0 alert
ADMET	Absorption Caco2 [h] (10^{-6} cm/s)	HIA[i]%	Distribution BBB[j] (log BB)		Metabolism CYP2D6[k] substrate	CYP1A2[l] inhibitor	Excretion Total Clearance (mL/min/kg)		Toxicity Hepato-toxicity[m]	
3a	0.894	92.97	−0.53		No	Yes	0.53		No	
3d	0.901	92.43	−0.50		No	Yes	0.51		No	
3f	1.351	91.51	−0.27		No	Yes	0.62		No	

a: Molecular weight, b: Topological Polar Surface Area, c: number of Rotable Bonds, d,d`: logarithm of partition coefficient of compound between n-octanol and water, e: number of hydrogen bond acceptors, f: number of hydrogen bond donors, g: Pan Assay Interference Structures, h: colon adenocarcinoma, i: Human Intestinal Absorption, j: Blood-Brain Barrier permeability, k: Cytochrome P450 2D6 inhibitor, l: Cytochrome P450 1A2 inhibitor, m: Hepatic toxicity.

with key amino acids in the AChE active site, compounds **3d** and **3f** appears as potential candidates for AChE inhibition activity. The best docking conformations of compounds **3** and references (Tacrine and Donepezil) are shown into BuChE and AChE active sites (Fig. 18).

2.4. ADMET properties

A computational study was performed to determine the ADMET properties of the three candidates **3a, 3d** and **3f** using the SwissADME and pkCSM-pharmacokinetics servers [73,74]. According to the results achieved reported in Table 7, the three tested compounds have some physicochemical properties in common. In fact, their molecular weights are inferior than 500 g/mol, they contain less than 5 H-bond donors and 10 H-bond acceptors. Also, they exhibit TPSA (Topological Polar Surface Area see https://en.wikipedia.org/wiki/Polar_surface_area) values less than 140 Å^2. In addition, the logarithm of the partition coefficient of compound between *n*-octanol and water MLogP and WLogP values are under 5 and the nROTB (number of Rotable Bonds) values are below 11. Based on these results, the three tested hydrazones meet Lipinski's rule of five [75], Veber's [76] and Egan's [77] rules with zero violations and no pan-assay interference structures (PAINS) alerts were detected.

Furthermore, the ADMET-absorption was evaluated and is presented in Table 7. The Caco-2 cell permeability is an indication of intestinal absorption [78]. Values obtained for all compounds ranged between 0.894 0.10^{-6} and 1.351 0.10^{-6} cm/s, indicating good permeability. Human intestinal absorption (HIA) values varied from 91.51 to 92.97 % (> 80 %) showing that compounds can have a high gastro-intestinal permeation. As seen in the ADMET- distribution section, The Blood Brain Barrier (BBB) permeability values of our compounds were predicted to range from −0.53 to −0.27 with log BB > −1 indicating that they are BBB permeable [79]. Metabolism-prediction was estimated according to the inhibition of the cytochrome P450 (CYP) superfamily of enzymes. In fact, CYP inhibition may cause toxicity or lack of efficacy for a drug [80]. The results reported in Table 7 indicate that molecules **3a, 3d** and **3f** were predicted to likely inhibit CYP1A2. In contrast, they were predicted to not inhibit CYP2D6. Excretion values were evaluated using the total clearance descriptor. Values ranged from 0.51 to 0.62 mL/min/kg (< 5 mL/min/kg). The toxicity level was predicted to assess hepatotoxicity. None of the candidates was found to cause liver damage.

3. Experimental

3.1. Apparatus and general information

NMR spectra were recorded on 300 and 400 MHz Brucker spectrometers. Chemical shifts were reported in ppm relative to the residual solvent peak (7.27 ppm for $CHCl_3$) for ^{1}H spectra, (77.00 ppm for $CDCl_3$) for ^{13}C spectra and referenced to H_3PO_4 for the ^{31}P spectra. The multiplicity of signals is indicated by the following abbreviations: s (singlet), d (doublet), m (multiplet). Column chromatography separations were performed using silica gel (0.040–0.060 mm). Infrared spectra were obtained with a Shimadzu IRS Spirit spectrometer using ATR technique in the 4000–400 cm^{-1} range.

3.2. General procedure of the synthesis of 1-(5,5-dialkyl-2-oxo-1,3,2-dioxaphosphoranyl)-propa-1,2-diene **2a-f**

In an ice bath, A mixture of propargylic alcohol (1.5. $10^{-}2$ mol) and triethylamine (1.6. 10^{-2} mol, 2.16 mL) in 100 mL of anhydrous THF was added to a three-neck oven dried round bottom flask and maintained at 0 °C. Next, a solution of 2-chloro-5,5-dialkyl-1,3,2-dioxaphosphorinane **1** (1.5. 10^{-2} mol) was added dropwise using an addition funnel. When all the reagent **1** was added, a white precipitate of triethylamine hydrochloride appears, and the reaction mixture was allowed to stir for 1 h at room temperature. After that, the resulting mixture was heated in THF under reflux for 1 h. The triethylamine hydrochloride was removed by filtration and THF was evaporated *in vacuo*. A resulting white solid was obtained and washed by hexane to afford the final compound.

Allenylphosphonates **2d, 2e** were synthesized according to literature procedures [22,23].

1-(5-methyl-5-propyl-2-oxo-1,3,2-dioxaphosphoranyl-3-phenyl-prop-1,2-diene) (2a)

M = 292.00 g/mol, Yield = (3.67 g, 12.6 mmol, 84 %), White solid, mp. (°C ± 2) = 116 °C. *Cis/Trans* ratio 27: 73, Diastereomer *Cis*: ^{31}P NMR: δ ^{31}P = 6.67, ^{1}H NMR: δ ^{1}H = 0.69 (s, 3H, CH3-C), 0.88 (t, 3H, CH_3-CH_2-CH_2), 1.18 (m, 2H, C-CH_2), 1.26 (m, 2H, C-CH_2-CH_2), 3.82–4.08 (m, 4H, $[AB]_2$), 5.76 (d, 1H, $^4J_{PH}$ =6.7 Hz, =CH-C6H5), 6.44 (dd, $^2J_{PH}$ = 13.3 Hz, $^4J_{HH}$ = 6.7 Hz, P-CH=), 7.16 (m, 5H, arom-H). ^{13}C NMR: δ ^{13}C= 14.3 (s, CH_3-CH_2-CH_2), 16.5 (s, CH2-CH2-C), 17.7 (s, CH_3-C), 35.1 (d, $^3J_{PC}$ = 6.4 Hz, -C-), 35.8 (s, CH_2-C), 75.5 (d, $^2J_{PC}$ = 6.6 Hz, CH2-O-P), 75.9 (d, $^2J_{PC}$ = 6.8 Hz, CH_2-O-P), 81.7 (s, P-CH=), 95.9 (d, $^3J_{PC}$ = 16.6 Hz, =CH-C_6H_5), 127.2 (d, $^6J_{PC}$ = 2.7 Hz, CH=$_{arom}$), 128.1 (d, $^7J_{PC}$ = 1.8 Hz, CH=$_{arom}$), 129.1 (d, $^5J_{PC}$ = 1.6 Hz, CH=$_{arom}$), 131.0 (d, $^4J_{PC}$ = 8.5 Hz, CH=$_{arom}$), 213.2 (d, $^2J_{PC}$= 1.8 Hz, =C=).

Diastereomer *trans*: ^{31}P NMR: δ ^{31}P = 7.4, ^{1}H NMR: δ ^{1}H = 0.74 (t,3H, CH_3-CH_2-CH_2), 0.89 (t, 2H, CH_3-CH_2-CH_2), 1.07 (s, 3H, CH_3-C), 1.10 (m, 2H, C-CH_2-CH_2), 3.90–4.01 (m, 4H, $[AB]_2$), 5.76 (d, 1H, $^4J_{PH}$ = 6.7 Hz, =CH-C_6H_5), 6.44 (dd, $^2J_{PH}$ = 13.3 Hz, $^4J_{HH}$ = 6.7 Hz, P-CH=), 7.18 (m, 5H, arom-H). ^{13}C NMR: δ ^{13}C = 14.6 (s, CH_3-CH_2-CH_2), 16.2 (s, CH_2-CH_2-C), 19.0 (s, CH_3-C), 35.1 (d, $^3J_{PC}$ = 6.3 Hz, -C-), 36.7 (s, -CH_2-C-

), 75.8 (d, $^{2}J_{PC}$ = 6.6 Hz, CH_2-O-P), 76.3 (d, $^{2}J_{PC}$ = 6.8 Hz, CH_2-O-P), 81.8 (s, P-CH=), 95.9 (d, $^{3}J_{PC}$ = 16.6 Hz, =CH-C_6H_5), 127.2 (d, $^{6}J_{PC}$ = 2.7 Hz, CH=$_{arom}$), 128.1(d, $^{7}J_{PC}$ = 1.8 Hz, CH=$_{arom}$), 128.9 (d, $^{5}J_{PC}$ = 1.6 Hz, CH=$_{arom}$),131.0 (d, $^{4}J_{PC}$ = 8.5 Hz, CH=$_{arom}$), 213.4 (d, $^{2}J_{PC}$ = 1.9 Hz, =C=). GC–MS: *m/z* = 292 [*M*+], 196 [(O)P(OH)$_2$-HC=C=CH-Ph], 178 [O-P(O)-CH=C=CH-Ph], 115 [Ph-CH=C=CH], 89 [P(=*O*)-O-CH_2-C], 69 [CH_2-CH-CH_2-CH_2-CH_3], 55 [CH_3-C-CH_2-CH_2], 41 [CH_3-C-CH_2]. IR-ATR (cm^{-1}): 2973, 1948, 1468, 1269, 1064, 1008, 975, 815, 538, 460 cm^{-1}.

1-(2-oxo-1,3,2-dioxapohosphoranyl-3,3-dimethylprop-1,2-diene) (2b)

M = 188.16 g/mol, Yield = (2.11 g, 11.21 mmol, 75 %), White solid, mp. (°C ± 2) = 49 °C, ^{31}P NMR: δ ^{31}P = 9.6, ^{1}H NMR: δ ^{1}H = 1.71 (d, 3H, Me), δ = 1.74 (d, 3H, Me), (2.12–2.24) (m, 2H, CH2-CH2-O), (4.21-4.44) (m, 4H, (CH_2-O)$_{Cycl}$), (5.13–5.17) (m, P-CH=). ^{13}C NMR: δ ^{13}C = 19.2 (d,$^{4}J_{PC}$ = 6.7 Hz, Me), 26.4 (d, $^{3}J_{PC}$ = 8.2 Hz, -CH_2-), 67.6 (d, $^{2}J_{CP}$ = 6.7 Hz, CH2-O-P), 76.6 (d, $^{1}J_{PC}$ = 192.1 Hz, P-CH=), 97.3 (d, $^{3}J_{PC}$ = 17.2 Hz, =C), 210.1 (s, =C=). IR-ATR (cm^{-1}): 2973, 1950, 1475, 1269, 1064, 1008, 815, 538, 460 cm^{-1}.

1-(2-oxo-1,3,2-dioxapohosphoranyl-3-phenylprop-1,2-diene (2c)

M = 236.21 g/mol, Yield = (2.76 g, 11.70 mmol, 78 %), White solid, mp. (°C ± 2) = 60 °C, ^{31}P NMR: δ ^{31}P = 7.6, ^{1}H NMR: δ ^{1}H = (2.13–2.24) (m, 2H, CH2-CH2-O), 2.44 (s, 3H, CH_3), (4.27- 4.39) (m, 4H, (CH_2-O)$_{Cycl}$), (5.70–5.75) (m, 1H, P-CH=), 7.16 (m, 5H, arom-H). ^{13}C NMR: δ ^{13}C= 16.0 (s, CH_3), 26.5 (d, $^{3}J_{PC}$ = 8.3 Hz, -CH_2-), 67.7 (d, $^{2}J_{CP}$ = 7.0 Hz, =CH-P), 79.9 (s, CH_2-O-P), 82.5 (s, CH_2-O-P), 102.5 (d, $^{3}J_{PC}$ = 17.3, =C-Ph), (125.9–133.9) (m, Ph), 213.3 (s, =C=).

1-(5,5-dimethyl-2-oxo-1,3,2-dioxaphosphoranyl-3-phenylprop-1,2-diene) (2d)

M = 264.26 g/mol, Yield = (2.85 g, 10.80 mmol, 72 %), White solid, mp. (°C ± 2) = 104 °C. ^{31}P NMR: δ ^{31}P = 6.5, ^{1}H NMR: δ ^{1}H = 0.86 (s, 3H, Me), 1.21 (s, 3H, Me), 3.94–4.07 (m, 4H, [AB]$_2$), 5.80 (d, $^{4}J_{PH}$ =6.7 Hz, 1H, =CH-C_6H_5), (6.49–6.55) (dd, 1H, $^{2}J_{PH}$ = 12.0 Hz, $^{4}J_{HH}$ = 6.0 Hz =CH-P), (7.28–7.38) (m, 5H, Ph). ^{13}C NMR: δ ^{13}C= 20.8 (s, CH_{3ax}), 21.7 (s, CH_{3eq}), 23.3 (s, CH_{2ax}), 32.4 (d, $^{3}J_{PC}$ = 6.7 Hz, -C-), 76.8 (d, $^{1}J_{PC}$ = 6.7, =CH-P), 81.51 (s, CH_2O-P), 84.04 (s, CH_2O-P), 95.9 (d, $^{3}J_{PC}$ = 16.5, =CH-Ph), (127.23–131.05) (m, Ph), 213.3 (s, =C=). IR-ATR (cm^{-1}): 2973, 1941, 1470, 1269, 1064, 1008, 975, 815, 538, 460 cm^{-1}.

1-(5,5-diethyl-2-oxo-1,3,2-dioxaphosphoranyl-3-phenylprop-1,2-diene) (2e)

M = 292.00 g/mol, Yield = (2.76 g, 13.50 mmol, 90%), White solid, mp. (°C ± 2) = 114°C. ^{31}P NMR: δ ^{31}P = 7.4, ^{1}H NMR: δ^{1}H = 0.75 (t, 3H, CH_3CH_2), 0.87 (t, 3H, CH_3-CH_2), 1.24 (m, 2H, CH_2-C), 1.60 (m, 2H, CH_2-C), 3.93–4.19 (m, 4H, [AB]$_2$), 5.80 (d, 1H, $^{4}J_{PH}$ = 6.8 Hz, =CH-C_6H_5), 6.47 (dd, $^{2}J_{PH}$ = 13.3 Hz, $^{4}J_{HH}$ = 6.5 Hz, P-CH=), 7.30 (m, 5H, arom-H). ^{13}C NMR: δ ^{13}C= 7.1 (s, CH_{3ax}), 7.2 (s, CH_{3eq}), 23.2 (s, CH_{2ax}), 23.5 (s, CH_{2eq}), 37.7 (d, $^{3}J_{PC}$ = 5.9 Hz, -C-), 74.2 (d, $^{2}J_{PC}$ = 6.8 Hz, C CH_2-O-P), 83.2 (d, $^{1}J_{PC}$ = 192.2 Hz, P-CH=), 96.0 (d, $^{3}J_{PC}$ = 16.7 Hz, =CH-C_6H_5), 127.4 (d, $^{5}J_{PC}$ = 2.8 Hz, C-O), 129.1 (d, $^{7}J_{PC}$ = 1.6 Hz, C-p), 214.2 (s, =C=).

1-(5,5-diethyl-2-oxo-1,3,2-dioxaphosphoranyl-3,3-dimethyl-prop-1,2-diene) (2f)

M = 244 g/mol, Yield = (2.63 g, 10.80 mmol, 72 %), White solid, mp. (°C ± 2) =110°C, ^{31}P NMR: δ ^{31}P = 11.2, ^{1}H NMR : δ ^{1}H = 0.75 (m, 3H, CH_3CH_2), 0.81 (m, 3H, CH_3CH_2), 1.25 (m, 2H, CH_2-C), 1.56 (m, 2H, CH_2-C), 1.71 (d, $^{5}J_{PH}$ = 4.0 Hz, 3H, C-CH_3), 1.73 (d, $^{5}J_{PH}$ = 4.0 Hz, 3H, C-CH_3)), 3.47–4.10 (m, 4H, [AB]$_2$), 5.14 (m, P-CH=), ^{13}C NMR: δ ^{13}C = 7.1 (s, CH_{3ax}), 7.2 (s, CH_{3eq}), 19.1 (s, CH_{2ax}), 22.2 (s, CH_{2eq}), 22.5 (s, Me), 23.0 (s, Me), 37.3 (d, $^{3}J_{PC}$ = 6.0 Hz, -C-), 73.8 (d, $^{2}J_{PC}$ = 7.0 Hz, CH_2-O-P), 75.2 (d, $^{1}J_{PC}$ = 202.0 Hz, P-CH=), 97.3 (d, $^{3}J_{PC}$ = 16.1 Hz, =C-CH_3), 210.9 (s, =C=).

3.3. General procedure of the synthesis of β-cycloalkoxyphosphonated hydrazones **3a-f**

To a solution of allenylphosphonate (10^{-3} mol) in 20 mL of $CHCl_3$, 10^{-3} mol of the respective hydrazine derivative was added dropwise at room temperature. The mixture was stirred for 20 min. Then, the solution was heated at 62 °C for 40 min-6 h. After concentration under reduced pressure, the crude material was washed by a 50:50 hexane/ether mixture. Hydrazones **3d, 3e** were synthesized according to literature procedures [22,23].

1-(5-methyl-5-propyl-2-oxo-1,3,2-dioxaphosphorany)-3-phenylpropanone (3a)

M = 324.36 g/mol. Yield = (0.24 g, 0.74 mmol, 74 %), White solid, mp. (°C ± 2) = 160 °C, 3a$_1$ (*Z/ E)* ratio 61: 39, 3a$_2$ (*Z/E*) ration 57: 43, ^{31}P NMR: δ ^{31}P$_1$= 21.12 *δ* ^{31}P$_2$ = 21.37, δ ^{31}P$_3$ = 21.55, δ ^{31}P$_4$ = 21.69, ^{1}H NMR: δ^{1}H = [0.82–0.86] (s,3H, CH_3-C), [0.90–0.96] (m, 3H, CH_3-CH_2-CH_2), [1.16–1.24] (m, 2H, C-CH_2), [1.25–1.34] (m, 2H, C- C CH_2-CH_2), [2.72–2.83] (d, 2H, P-CH_2), 3.50 (s, 2H, CH_2- Ph), [3.65–4.18] (m, 4H, [AB]$_2$), [5.19–5.60] (s, 2H, NH_2), [7.11–7.25] (m, 5H, Ph), ^{13}C NMR: δ ^{13}C= [14.6–14.9] (CH_3-CH_2-CH_2), [16.1–16.6] (CH_2CH_2C), [18.2–18.8] (CH_3-C), [24.2–26.1] (CH_2-P), 35.1 (-C-), 36.5 (-CH_2-C-), 44.3 (CH_2-Ph), 73.7 (CH_2-O-P), 74.5 (CH_2-O-P), 126.9–137.4 (Ph) [143.0–146.2] (CN). GC–MS: *m/z* = 324 [*M*$^+$], 130 [(CH_3-CH_2) (CH_3) C (CH_2O)$_2$], 103 [C_6H_5-CH_2-C], 91 [C_6H_5-CH_2], 55 [CH_3-C(CH_2)-CH_2]. IR-ATR (cm^{-1}): 3478, 2960, 1650, 1500, 1265, 696, 1006, 527 cm^{-1}.

1-(2-oxo-1,3,2-dioxaphosphoranyl)−3,3-dimethylpropanone (3b)

M = 220.21 g/mol, Yield = (0.17 g, 0.80 mmol, 80 %), Pasty solid, Z/E ratio 96: 4, *Z* isomer: ^{31}P NMR: δ ^{31}P = 21.5, ^{1}H NMR: δ ^{1}H = 1.11 (d, 6H, CH_3), 1.63 (m, 1H, -CH-CH_3), 1.68 (m, 2H, CH_2-CH_2-O), 3.17 (d, 2H, $^{2}J_{PH}$ = 22.3 Hz, CH_2-P), 4.07–4.38 (m, 4H, (CH_2-O)$_{Cycl}$), 7.31(s, 2H, NH_2), ^{13}C NMR: δ ^{13}C = 20.1 (s, Me), 25.1 (CH_2-CH_2-O), 26.4 (d, $^{1}J_{PC}$ = 7.5 Hz, P-CH_2), 36.2 (CH-Me), 66.2 (d, $^{2}J_{PC}$ = 6.7 Hz, CH_2-O-P), 149.1 (d, $^{2}J_{PC}$ =11.3 Hz, CN). *E* isomer: ^{31}P NMR: δ ^{31}P = 21.4, ^{1}H NMR: δ^{1}H=1.18 (d, 6H, CH_3), 1.85 (m, 1H, -CH-CH_3), 1.85 (m, 2H, CH_2-CH_2-O), 2.18 (d, 2H, $^{2}J_{PH}$ = 8.3 Hz, CH_2-P), 3.80–3.95 (m, 4H, (CH_2-O)$_{Cycl}$), 7.24 (s, 2H, NH_2). ^{13}C NMR: δ ^{13}C = 20.1 (s, Me), 25.1 (CH_2-CH_2-O), 26.4 (d, $^{1}J_{PC}$ = 7.5 Hz, P-CH_2), 36.2 (CH-Me), 66.2 (d, $^{2}J_{PC}$ = 6.7 Hz, CH_2-O-P), 149.1 (d, $^{2}J_{PC}$ = 11.3 Hz, CN).

1-(2-oxo-1,3,2-dioxaphosphoranyl)−3-phenylpropanone (3c)

M = 282.11 g/mol. Yield = (0.21 g, 0.75 mmol, 75 %), White crystal, mp. (°C ± 2) = 170 °C, Z/E ratio 100: 0, *Z* isomer: ^{31}P NMR: δ ^{31}P = 20.8, ^{1}H NMR: δ^{1}H = 1.34 (d, 3H, CH_3), 1.94 (m, 2H, CH_2-CH_2-O), 2.51 (dd, $^{2}J_{PH}$ = 24.0 Hz, $^{2}J_{HH}$ = 15.0 Hz,1H, CH-P), 2.86 (dd, $^{2}J_{PH}$ 24.0 Hz, $^{2}J_{HH}$ 15.0 Hz,1H, CH-P), 3.57 (m, 1H, CH-CH_3), (4.01–4.54) (m, 4H, (CH_2-O)$_{Cycl}$), 5.62 (s, 2H, NH_2), (7.08–7.27) (m, 5H, Ph), ^{13}C NMR: δ ^{13}C = 19.6 (s, CH3), 25.5 (s, CH_2-CH_2-O), 26.3 (d, $^{1}J_{PC}$ = 7.7 Hz, P-CH_2), 47.7 (s, HC—CH_3), 66.5 (dd, $^{2}J_{PC}$ = 1.8 Hz, CH_2-O-P), (126.6–143.2) (m, Ph), 146.1 (d, $^{2}J_{PC}$ = 10.9 Hz, CN). GC–MS: *m/z* = 282 [*M*$^+$], 144 [Ph-CH-C(C)=N-NH_2] 105 [CH_2-CH_2-O-P-O-CH_2], 91 [CH_2-O-P-O-CH_2], 77 [Ph], 44 [CH_2-CH_2-O]. IR-ATR (cm^{-1}): 3300, 2950, 1633, 1500, 1266, 1054, 515 cm^{-1}.

1-(5,5-dimethyl-2-oxo-1,3,2-dioxaphosphorany)−3-phenylpropanone (3d)

M = 296.31 g/mol, Yield = (0.21 g, 0.70 mmol, 70 %), White solid, mp. (°C ± 2) = 150 °C, Z/E ratio 86:14, *Z* isomer: ^{31}P NMR: δ ^{31}P = 21.0, ^{1}H NMR: δ^{1}H = 0.92 (s, 3H, CH_3), 1.04 (s, 3H, CH_3), 2.75 (d, $^{2}J_{PH}$ = 24.0 Hz, 2H, P-CH_2),3.54 (s, 2H, CH_2-Ph), 3.70–4.20 (m, 4H, [AB]$_2$), 5.62 (s, 2H, NH_2), 7.14–7.6 (m, 5H, Ph). ^{13}C NMR: δ ^{13}C = 21.1 (s, CH_{3e}), 21.8 (s, CH_{3a}), 24.3 (d, $^{1}J_{PC}$ = 126.03 Hz, P-CH_2), 32.5 (d, $^{3}J_{PC}$ = 5.8, C-Me_2), 44.3 (s, CH_2-Ph), 75.0 (d, $^{2}J_{PC}$ = 6.3 Hz, CH_2O-P), 126.0–136.2 (m, Ph), 161.7 (d, $^{2}J_{PC}$ = 3.0 Hz, CN). *E* isomer: ^{31}P NMR: δ ^{31}P = 21.9, ^{1}H NMR: δ^{1}H = 1.11 (s, 3H, CH_3), 1.14 (s, 3H, CH_3), 2.82 (d, $^{2}J_{PH}$ =24.0 Hz, 2H, P-CH_2), 3.48 (s, 2H, CH_2-Ph), 3.70–4.21 (m, 4H, [AB]$_2$), 5.24 (s, 2H, NH_2), 7.13–8.25 (m, 5H, Ph). ^{13}C NMR: δ ^{13}C = 21.4 (s, CH_{3e}), 21.4 (s, CH_{3a}), 26.3 (d, $^{1}J_{PC}$ = 127,04 Hz, P-CH_2), 32.2 (d, $^{3}J_{PC}$

= 7.0, C-Me$_2$), 43.6 (s, CH$_2$-Ph), 75.7 (d, $^2J_{PC}$ = 6.9 Hz, CH$_2$-O-P), 126.0–136.1 (m, Ph), 169.91(d, $^2J_{PC}$ = 3.0 Hz, CN). GC–MS: *m/z* = 234 [C(CH$_2$-O)$_2$-P-CH$_2$-C(N)-CH$_2$-Ph], 219 [(Me)$_2$C(CH$_2$-O)$_2$-P(O)-CH$_2$-C(CH$_2$)=N-NH$_2$], 173 [(Me)$_2$C(CH$_2$-O)$_2$-P-CH$_2$-C=N], 91 [C$_6$H$_5$-CH$_2$], 77 [Ph], 65 [P(OH)$_2$], 41 [CH$_3$-C-CH$_2$]. IR-ATR (cm^{-1}): 3300, 2973, 1633, 1490, 1266, 1054, 515 cm^{-1}.

1-(5,5-diethyl-2-oxo-1,3,2-dioxaphosphoranyl)−3-phenyl-propanone (3e)

M = 324.00 g/mol, Yield = (0.23 g, 0.70 mmol, 70 %), White solid, mp. (°C ± 2) = 138°C, Z/E ratio 62: 38, *Cis (Z)* isomer: ^{31}P NMR: δ ^{31}P = 21.6, ^{1}H NMR: δ^{1}H = 0.99 (m, 3H, CH$_3$C), 1.10 (m,3H, CH$_3$-C), 1.30 (m, 2H, C-CH$_2$), 1.31 (m, 2H, CH$_2$-C), 2.82 (d, $^3J_{PH}$ =12.6 Hz, CH$_2$-CN), 3.61 (d, $^2J_{PH}$ = 2.50 Hz, P-CH$_2$), 3.82–4.00 (m, 4H, [AB]$_2$), 5.58 (s, 2H, NH$_2$), 7.20 (m, 5H, arom-H). ^{13}C NMR: δ ^{13}C = 6.9 (CH$_3$-C), 7.1 (CH$_3$-C), 22.5 (C-CH$_2$), 23.1 (C-CH$_2$), 25.2 (CH$_2$-Ph), 29.0 (P-CH$_2$), 37.5 (-C-), 73.1 (d, $^2J_{PC}$ = 6.4 Hz, CH$_2$-O-P), 113.0–128.5 (CH-arom), 128.8 (d, $^5J_{PC}$ = 4.6 Hz, C-i), 145.7 (CN).

Trans (E) isomer: ^{31}P NMR: δ ^{31}P = 21.8. ^{1}H NMR: δ^{1}H = 0.82 (m, 3H, CH$_3$C), 0.88 (m, 3H, CH$_3$-C), 1.50 (m, 2H, CH$_2$), 1.52 (m, 2H, CH$_2$), 2.90 (d, $^3J_{PH}$ =11.3, CH$_2$-CN), 3.73 (d, $^2J_{PH}$ = 1.8 Hz, 2H, P-CH$_2$), 4.17–4.26 (m, 4H, [AB]$_2$), 5.58 (s, 2H, NH$_2$), 7.32 (m, 5H, arom-H). ^{13}C NMR: δ ^{13}C = 7.0 (CH$_3$-C), 7.1 (CH$_3$-C), 22.8 (C-CH$_2$), 23.1 (C-CH$_2$), 25.2 (CH$_2$-Ph), 29.0 (P-CH$_2$), 37.5(-C-), 73.1(d, $^2J_{PC}$ = 6.4 Hz, CH$_2$-O-P), 113.0–128.5 (CH-arom), 129.6 (d, $^5J_{PC}$ = 11.2 Hz, C-i), 145.7 (CN). GC–MS: *m/z*: 324 (M^+), 130 (Et$_2$C(CH$_2$O)$_2$), 103 (C$_6$H$_5$-CH$_2$-C), 91 (C$_6$H$_5$-CH$_2$), 55 ((CH3)$_2$C=CH). IR-ATR (cm^{-1}): 3200, 2980, 1633, 1490, 1054, 500 cm^{-1}.

1-(5,5-diethyl-2-oxo-1,3,2-dioxaphosphoranyl)-N-methyl-3-phenylpropanone (3f)

M = 338.00 g/mol, Yield = (0.27 g, 0.80 mmol, 80%), White solid, mp. (°C ± 2) = 108°C, Z/E ratio 85: 15, *Cis (Z)* isomer: ^{31}P NMR: δ ^{31}P = 21.3, ^{1}H NMR: δ ^{1}H = 0.80 (m, 3H, CH$_3$-C), 0.84 (m, 3H, CH$_3$-C), 1.32 (m, 2H, C-CH$_2$), 1.41 (m, 2H, C-CH$_2$), 2.72 (s, Me), 3.08 (s, CH$_2$-CN), 3.61 (d, $^2J_{PH}$ = 2.3 Hz, P-CH$_2$), 3.74–4.32 (m, 4H, [AB]$_2$), 5.56 (s, 1H, NH), 7.20 (m, 5H, arom-H). ^{13}C NMR: δ ^{13}C = 4.8 (CH$_3$-C), 5.0 (CH$_3$-C), 22.4 (C-CH$_2$), 23.1 (C-CH$_2$), 25.2 (CH$_2$-CN), 30.0 (P-CH$_2$), 30.7 (Me), 37.6 (-C-), 43.8 (CH2-Ph) 73.0 (CH$_2$-O-P), 126.3–137.4 (C$_{arom}$), 139.8 (CN).

Trans (E) isomer: ^{31}P NMR: δ ^{31}P = 21.7 ^{1}H NMR: δ ^{1}H = 0.83 (m,3H, CH$_3$-C), 0.88 (m,3H, CH$_3$-C), 1.34 (m, 2H, C-CH$_2$), 1.47 (m, 2H, C-CH$_2$), 2.78 (s, Me), 3.10 (s, CH$_2$-CN), 3.61 (d, $^2J_{PH}$ = 2,3 Hz, P-CH$_2$), 3.82–4.27 (m, 4H, [AB]$_2$), 5.59 (s, 1H, NH), 7.78 (m, 5H, arom-H). ^{13}C NMR: δ ^{13}C = 4.9 (CH$_3$-C), 5.1 (CH$_3$-C), 22.5 (C-CH$_2$), 23.2 (C-CH$_2$), 25.3 (CH$_2$-CN), 30.1 (P-CH$_2$), 30.8 (Me), 37.7 (-C-), 43.9 (CH2-Ph), 73.1 (CH$_2$-O-P), 126.3–137.4 (C$_{arom}$), 139.9 (CN).

3.4. Theoretical calculations

All computations were performed with the Gaussian 09 program [81,82]. The Conformations were optimized using DFT geometry optimizations using hybrid B3LYP [83] functional and the 6311++ *G* (d, p) basis set. To be sure that all optimized structures lay at a local point on the potential energy surface, harmonic vibrational frequencies of all structures were performed. None of the predicted spectra has any imaginary frequencies.

3.5. General X-ray structure analysis and refinement

Data collection was performed on a Bruker D8 Venture four-circle diffractometer from Bruker AXS GmbH (Karlsruhe, Germany). CPAD detectors used were Photon II from Bruker AXS GmbH; X-ray sources: Microfocus source IμS; and microfocus source IμS Mo and Cu, respectively, from Incoatec GmbH with mirror optics HELIOS and a single hole collimator from Bruker AXS GmbH. Programs used for data collection were APEX4 Suite (v2021.10–0) and integrated programs SAINT (V8.40B; integration) and SADABS (2016/2; Bruker, 2016/2 absorption correction) from Bruker AXS GmbH [84]. The SHELX programs were used for further processing [85]. The solution of the crystal structures was done with the help of the program SHELXT [86], the structure refinement with SHELXL [87]. The processing and finalization of the crystal structure data was done with program OLEX2 v1.5 [88]. All non-hydrogen atoms were refined anisotropically. For the hydrogen atoms, the standard values of the SHELXL program were used with U_{iso}(H) = –1.2 U_{eq}(C) for CH$_2$ and CH and with U_{iso}(H) = –1.5 U_{eq}(C) for CH$_3$. All H atoms were refined freely using independent values for each U_{iso}(H).

Crystal data for C$_{13}$H$_{19}$FN$_2$O$_3$P (**3c**), M = 282.27 g. mol^{-1}, colorless blocks, crystal size 0.415 × 0.326 × 0.117 mm^3, monoclinic, space group $P2_1/c$, a = 5.9823(4) Å, b = 7.5563(5) Å, c = 30.729(2), α = 90°, β = 94.802 (2)°, γ = 90°; V = 1384.19(16) Å^3, Z = 4, D_{calc} = 1.355 g/cm^3, T = 100 K, R_1 = 0.0388, wR_2 = 0.0972 for 195,798 reflections with $I \geq 2\sigma$ (I) and 7495 independent reflections. GOF = 1.110. Largest diff. peak/hole/e Å^{-3} 0.53/–0.39.

Crystal data for C$_{16}$H$_{23}$FNO$_3$P (**4**), M = 308.32 g. mol^{-1}, colorless needles, crystal size 0.382 × 0.092 × 0.063 mm^3, monoclinic, space group $P2_1/c$, a = 10.89(3) Å, b = 6.113(11) Å, c = 25.02(7), α = 90°, β = 97.36 (12)°, γ = 90°; V = 1651(7) Å^3, Z = 4, D_{calc} = 1.240 g/cm^3, T = 100 K, R_1 = 0.0666, wR_2 = 0.1902 for 12,302 reflections with $I \geq 2\sigma$ (I) and 3246 independent reflections. GOF = 1.047. Largest diff. peak/hole/e Å^{-3} 0.42/–0.48. Other crystallographic data and structure refinement details for hydrazone **3c** and azine **4** are presented in Table S1.

Data were collected using graphite monochromated MoK$_\alpha$ radiation λ = 0.71073 Å and have been deposited at the Cambridge Crystallographic Data Centre as CCDC 2,323,102 (**3c**) and 2,333,377 (**4**). (Supplementary Materials). The data can be obtained free of charge from the Cambridge Crystallographic Data Centre via http://www.ccdc.cam.ac.uk/getstructures, accessed on 21 January 2024.

3.6. Molecular docking

The 3D crystal structures of PDB were obtained from the RSCB protein data bank: Butyrylchlinesterase (BuChE) in complex with Tacrine (PDB: 4BDS) [89], Acetylcholinesterase (AChE) in complex with Donepezil (PDB: 4EY7) [90] All water molecules were removed, hydrogen atoms were added before docking using Discovery Studio Visualizer D.S. (2017) (Biovia San Diego, CA, USA) Gasteiger charges were also added to the system during the preparation of the receptor input file. Docking studies were carried out using AutodockTools (ADT version 1.5.6) [71] to prepare enzyme and ligands files (PDBQT). The optimization of all the geometries was performed with ACD (3D viewer) software [91] Cocrystalized ligands into proteins were used as reference ligands and redocked int the active site for energy comparison. 2D pictures were captured using Discovery Studio Visualizer (2017) (Biovia San Diego, CA, USA).

In order to test the validation of the docking performance and the accuracy of co-crystallized ligands for both targets, Donepezil and Tacrine were re-docked into the binding site pocket of AChE and BuChE, respectively. Root-Mean-Square Deviation (RMSD) values between the docking and initial poses, docking scores, and properties of AChE and BuChE were given in Table 8.

Table 8
Information details related to proteins AChE and BuChE.

Proteins	Methods	Resolution (Å)	Amino acids number	Co-crystallized ligand	Docking score (Kcal/mol)	RMSD
4EY7	X-ray diffraction	2.35	542	Donepezil	−11.6	0.748
4BDS	X-ray diffraction	2.10	529	Tacrine	−8.1	0.469

The co-crystallized ligands of 4EY7 and 4BDS are: Donepezil (C_{24} H_{29} N O_3) and Tacrine (C_{13} H_{14} N_2) respectively.

3.7. ADME-Toxicity and drug-likeness prediction

ADMET properties (TPSA, n-ROTB, Log P, n-H bond donors and acceptors) were predicted using the SwissADME server (http://www.swissadme.ch/, accessed on 02 /05/2024) [73] in order to evaluate Lipinski, Vaber, Egan and PAINS filters. Moreover, the pkCSM server (https://biosig.unimelb.edu.au/pkcsm/prediction, accessed on 02/05/2024) [74] was employed to predict Absorption-, Distribution-, Metabolism-, Excretion- and Toxicity properties.

4. Conclusion

In the present work, we have prepared allenylphosphonates **2a-f** and β-cycloalkoxyphosphonated hydrazones **3a-f** bearing a dioxaphosphorinane ring. Most of them coexist in solution as diastereomeric mixtures. An attribution of the signals in the ^{31}P NMR spectra of allenylphosphonate **2a** and hydrazone **3a** to their corresponding diastereomers was attempted based on mechanistic elucidation and theoretical calculations. Unlike the other hydrazones, the ^{31}P NMR spectrum of the hydrazone **3c** displays only a singlet. X-ray diffraction was therefore conducted to understand this difference by investigating the structure of hydrazone **3c**. The analyzed single crystal shows a *Z* configuration stabilized by a strong intramolecular hydrogen bond. DFT calculation was conducted and confirmed that the *Z*-configuration is the more stable one, rationalizing the observation of a just singlet in the ^{31}P NMR spectrum. We have also found by serendipity that hydrazones **3** may serve as precursors of azines like **4**. The potential of this condensation will be further exploited in future studies. Also, the potential of compounds **3** and **4** acting as *N*-donor ligands in coordination chemistry deserves forthcoming investigations. The experimental IR spectrum of **3c** was compared with the computed one and found to fit well. Docking simulations performed on AChE and BuChE enzymes revealed that all hydrazones **3a-f** exhibit high affinity for the binding sites of AChE and BuChE. Compounds **3a** and **3d** were identified as very potent for BuChE enzyme inhibition. On the other hand, compounds **3d** and **3f** showed the highest affinity with the active site of AChE enzyme. The ADMET prediction revealed that hydrazones **3a, 3d** and **3f** exhibit drug- likeness according to Lipinski's, Veber's and Egan's rules. These *in silico* simulations allowed us to select the most promising candidates that will be the subject of *in vivo* experiments concerning AChE and BuChE inhibitory activity in a subsequent work.

CRediT authorship contribution statement

Dorra Kanzari-Mnallah: Writing – original draft, Software, Investigation, Formal analysis. **Sirine Salhi:** Investigation. **Michael Knorr:** Writing – review & editing, Writing – original draft, Project administration, Conceptualization. **Jan-Lukas Kirchhoff:** Software, Investigation. **Carsten Strohmann:** Resources, Data curation. **Med Lotfi Efrit:** Resources. **Azaiez Ben Akacha:** Conceptualization, Writing – review & editing.

Declaration of competing interest

The authors declare that they have no known competing financial interests or personal relationships that could have appeared to influence the work reported in this paper.

Data availability

Data will be made available on request.

Acknowledgements

This work was supported financially by the general directorate of scientific research, Tunisian ministry of scientific research.

Supplementary materials

Supplementary material associated with this article can be found, in the online version, at doi:10.1016/j.molstruc.2024.139035.

References

[1] G. Uppal, S. Bala, S. Kamboj, M. Saini, Therapeutic review exploring antimicrobial potential of hydrazones as promising lead. Der, Pharma. Chem. 3 (2011) 250–268.
[2] P. Krishnamoorthy, P. Sathyadevi, K. Senthilkumar, P.T. Multhiah, R. Damesh, N. Dharmaraj. Copper(I) hydrazone complexes: synthesis, structure, DNA binding, radicalscavenging and computational studies. Inorg. Chem. Commun. 14 (2011) 1318–1322. https://doi.org/10.1016/j.inoche.2011.05.004.
[3] Q. Mo, J. Deng, Y. Liu, G. Huang, Z. Li, P. Yu, Y. Gou, F. Yang, Mixed-ligand Cu(II) hydrazone complexes designed to enhance anticancer activity, Eur. J. Med. Chem. 156 (2018) 368–380, https://doi.org/10.1016/j.ejmech.2018.07.022.
[4] T.T. Adejumo, N.V. Tzouras, L.P. Zorba, D. Radanovic, A. Pevec, S. Grubišic, D. Mitic, K.K. Andelkovic, G.C. Vougioukalakis, B. Cobeljic, I. Turel, Synthesis, characterization, catalytic activity, and DFT calculations of Zn(II) hydrazone complexes, Molecules. 25 (2020) 4043–4061, https://doi.org/10.3390/molecules25184043.
[5] M. Gökçe, S. Utku, E. Küpeli, Synthesis and analgesic and anti-inflammatory activities 6-substituted-3(2H) pyridazinone-2-acetyl-2-(p-substituted/nonsubstituted benzal)hydrazone derivatives, Eur. J. Med. Chem. 44 (9) (2009) 3760–3764, https://doi.org/10.1016/j.ejmech.2009.04.048.
[6] R. Narang, B. Narasimhan, S. Sharma, A review on biological activities and chemical synthesis of hydrazide derivatives, Curr. Med. Chem. 19 (4) (2012) 569-612, https://doi.org/10.2174/092986712798918789.
[7] B.F. Abdel-Wahab, G.E.A. Awad, F.A. Badria, Synthesis, antimicrobial, antioxidant, antihemolytic and cytotoxic evaluation of new imidazole-based heterocycles, Eur. J. Med. Chem. 46 (5) (2011) 1505–1516, https://doi.org/10.1016/j.ejmech.2011.01.062.
[8] P. Dandawate, E. Khan, S. Padhye, H. Gaba, S. Sinha, J. Deshpande, K.V. Swamy, M. Khetmalas, A. Ahmad, F.H. Sarkar, Synthesis, characterization, molecular docking and cytotoxic activity of novel plumbagin hydrazones against breast cancer cells, Bioorg. Med. Chem. Lett. 22 (9) (2012) 3104–3108, https://doi.org/10.1016/j.bmcl.2012.03.060.
[9] J. Pandey, R. Pal, A. Dwivedi, K. Hajela, Synthesis of some new diaryl and triaryl hydrazone derivatives as possible estrogen receptor modulators, Arzneim. Forsch. 52 (1) (2002) 39–44, https://doi.org/10.1055/s-0031-1299854.
[10] A.H. Abadi, A.A.H. Eissa, G.S. Hassan, Synthesis of novel 1,3,4-trisubstituted pyrazole derivatives and their evaluation as antitumor and antiangiogenic agents, Chem. Pharm. Bull. 51 (7) (2003) 838–844, https://doi.org/10.1248/cpb.51.838.
[11] N. Terzioğlu, A. Gürsoy, Synthesis and anticancer evaluation of some new hydrazone derivatives of 2,6-dimethylimidazo[ˆ2,1-b] [1,3,4]thiadiazole-5-carbohydrazide, Eur. J. Med. Chem. 38 (7–8) (2003) 781–786, https://doi.org/10.1016/S0223-5234(03)00138-7.
[12] S.K. Sridhar, S.N. Pandeya, J.P. Stables, A. Ramesh, Anticonvulsant activity of hydrazones, Schiff and Mannich bases of isatin derivatives, Eur. J. Pharm. Sci. 16 (3) (2002) 129–132, https://doi.org/10.1016/S0928-0987(02)00077-5.
[13] A.A. Mohamed Eissa, G.A. Soliman, M.H. Khataibeh, Design, Synthesis and anti-inflammatory activity of structurally simple anthranilic acid congeners devoid of ulcerogenic side effects, Chem. Pharm. Bull. 60 (10) (2012) 1290–1300, https://doi.org/10.1248/cpb.c12-00516.
[14] I. Bozbey, Z. Ozdemir, H. Uslu, A.B. Ozcelik, F.S. Senol, I.E. Orhan, M. Uysal, A series of new hydrazone derivatives: synthesis, molecular docking and anticholinesterase activity studies, Mini. Rev. Med. Chem. 20 (11) (2020) 1042–1060, https://doi.org/10.2174/1389557519666191010154444.
[15] M. Prinz, S. Parlar, G. Bayraktar, V. Alptuzun, E. Erciyas, A. Fallarero, D. Karlsson, P. Vuorela, M. Burek, C. Forster, E. Turnc, G. Armagan, A. Yalcin, C. Sciller, K. Leuner, M. Krug, C.A. Sotriffer, U. Holzgrabe, 1,4-Substituted 4- (1H)-

pyridylene-hydrazone-type inhibitors of AChE, BuChE, and amyloid-β aggregation crossing the blood-brain barrier, Eur. J. Pharma. Sci. 49 (4) (2013) 603–613, https://doi.org/10.1016/j.ejps.2013.04.024.
[16] F. Yang, J. Zhao, G. Chen, H. Han, S. Hu, N. Wang, Y. Chen, Z. Zhou, B. Dai, Y. Hou, Y. Liu, Design, synthesis, and evaluation of hydrazones as dual inhibitors of ryanodine receptors and acetylcholinesterases for Alzheimer's disease, Bioorg. Chem. 133 (2023) 106432, https://doi.org/10.1016/j.bioorg.2023.106432.
[17] H. Hampel, M.M. Mesulam, A.C. Cuello, M.R. Farlow, E. Giacobini, G.T. Grossberg, A.S. Khachaturian, A. Vergallo, E. Cavedo, P.J. Snyder, Z.S. Khachaturian, The cholinergic system in the pathophysiology and treatment of Alzheimer's disease, Brain 141 (7) (2018) 1917–1933, https://doi.org/10.1093/brain/awy132.
[18] M. Mehta, A. Adem, M. Sabbagh, New Acetylcholinesterase Inhibitors for Alzheimer's Disease, Int. J. Alzheimers Dis. (2012) 1–8, https://doi.org/10.1155/2012/728983.
[19] P. Anand, B. Singh, A review on cholinesterase inhibitors for Alzheimer's disease, Arch. Pharm. Res. 36 (2013) 375–399, https://doi.org/10.1007/s12272-013-0036-3.
[20] A. Ben Akacha, N. Ayed, B. Baccar, Oxydes de diazaphospholines-1,2,3 : synthèse et etude spectrographique IR et de RMN ^{1}H, ^{31}P, ^{13}C. Phosphorus. Sulfur, Silicon. Relat. Elem. 55 (1991) 205–210, https://doi.org/10.1080/10426509108045942.
[21] A. Ben Akacha, S. Barkallah, H. Zantour, ^{13}C NMR and ^{31}P NMR spetral assignment of new β- phosphonylated hydrazones, Magn. Reson. Chem. 37 (12) (1999) 916–920, https://doi.org/10.1002/(SICI)1097-458X(199912)37:12<916::AID-MRC547>3.0.CO;2-W.
[22] N. Salah, Y. Arfaoui, M. Bahri, M.L. Efrit, A. Ben Akacha, Synthèse et etude conformationnelle par RMN (^{1}H, ^{13}C, ^{31}P) et DFT des cycloalcoxyphosphinallenes et des hydrazones β- cycloalcoxyphosphonatees. Phosphorus, Sulfur Silicon, Rel. Elem. 188 (2013) 609–622, https://doi.org/10.1080/10426507.2012.700348.
[23] D. Kanzari-Mnallah, M.L. Efrit, A. Ben Akacha, Synthèse de 1,3,2-dioxaphosphorinanes diastereoisomers : influence de la conformation des 1,3-diols de depart sur leurs structures et conformations, Phosphorus. Sulfur Silicon. Relat. Elem. 192 (6) (2017) 665–673, https://doi.org/10.1080/10426507.2017.1308931.
[24] A.P. Boiselle, N.A. Meinhardt, Acetylene-Allene rearrangements. Reactions of trivalent phosphorus chlorides with α-acetylenic alcohols and glycols, J. Org. Chem. 27 (1962) 1828–1833, https://doi.org/10.1021/jo01052a084.
[25] N.G. Khusainova, A.N. Pudovik, Phosphorylated Allenes. Method of synthesis and properties, Russ. Chem. Rev. 56 (6) (1987) 564–578, https://doi.org/10.1070/rc1987v056n06abeh003290.
[26] V. Mark, A facile S_Ni' rearrangement: the formation of 1,2-alkadienylphosphonates from 2-alkynyl phosphites, Tetrahedron. Lett. 3 (7) (1962) 281–285, https://doi.org/10.1016/S0040-4039(00)70867-7.
[27] D. Kanzari-Mnallah, M.L. Efrit, J. Pavlicek, F. Veilleux, H. Boughzala, A. Ben Akacha, Synthesis, conformational analysis and crystal structure of new thioxo, oxo, seleno, diastreomeric cyclophosphamides containing 1,3,2-dioxaphosphorinane, Curr. Org. Chem. 23 (2) (2019) 205–213, https://doi.org/10.2174/1385272823666190213142748.
[28] S. Cruz-Gregorio, V. Rodriguez-Palacios, H. Hopfl, L. Quintero, F. Sartillo-Piscil, Six-membered ring phosphates and phosphonates as model compounds for cyclic phosphate prodrugs: is the anomeric effect involved in the selective and spontaneous cleavage of cyclic phosphate prodrugs? J. Org. Chem. 74 (2009) 197–205, https://doi.org/10.1021/jo8017473.
[29] E. Juaristi, G. Cuevas, Recent studies of the anomeric effect, Tetrahedron. 48 (24) (1992) 5019–5087, https://doi.org/10.1016/S0040-4020(01)90118-8.
[30] The effect of salt formation on structure and charge distribution in imines. Part 4, Energy barriers to isomerisation about the C–N bond in 2,6-dimethyl-4-arylimino-pyrans and their salts: solvent and substituent effects, and evidence for isomerisation mechanisms. M. P. Sammes, J. Chem. Soc. Perkin Trans. 2 (1981) 1501–1507, https://doi.org/10.1039/P29810001501.
[31] R. Kinghat, G. Schmitt, K. Ciamala, A. Khatyr, M. Knorr, S. Jacquot-Rousseau, Y. Rousselin, M.M. Kubicki, 1,3-Dipolar cycloaddition of diaryldiazomethanes across N-ethoxy-carbonyl-N-(2,2,2-trichloroethylidene)amine and reactivity of the resulting 2-azabutadienes towards thiolates and cyclic amides, C. R. Chim. 19 (2016) 319–331, https://doi.org/10.1016/j.crci.2015.09.017.
[32] S.M. Landge, E. Tkatchouk, D. Benítez, D.A. Lanfranchi, M. Elhabiri, W.A. Goddard III, I. Aprahamian, Isomerization mechanism in hydrazone-based rotary switches: lateral shift, rotation, or tautomerization? J. Am. Chem. Soc. 133 (25) (2011) 9812–9823, https://doi.org/10.1021/ja200699v.
[33] J. Lasri, A.I. Ismail, Metal-free and FeCl3-catalyzed synthesis of azines and 3,5-diphenyl-1H-pyrazole from hydrazones and/or ketones monitored by high resolution ESI+-MS, Indian J. Chem. B57 (3) (2018) 362–373. http://nopr.niscair.res.in/handle/123456789/43824.
[34] R. Kinghat, A. Khatyr, G. Schmitt. M. Knorr, M.M. Kubicki, E. Vigier, F. Villafane, Mono- and di-nuclear 2,3-diazabutadiene and 2-azabutadiene complexes of Rhenium(I): syntheses, luminescence spectra and X-ray structures, Inorg. Chem. Commun. 11 (2008) 1061–1064, https://doi.org/10.1016/j.inoche.2008.05.022.
[35] S. Cruz-Gregorio, M. Sanchez, A. Clara-Sosa, S. Bernes, L. Quintero, F. Sartillo-Piscil, Intramolecular Hydrogen Bonding (P=O…H) Stabilizes the Chair Conformation of Six-Membered Ring Phosphates, J. Org. Chem. 70 (2005) 7107–7113, https://doi.org/10.1021/jo050753+.
[36] Y. Arfaoui, S. Kouass, N. Salah, A. Ben akacha, A. Guesmi, Ethyl 3-[1-(5,5-dimethyl-2-oxo-1,3,2-dioxaphosphorin-2-yl)propan-2-ylidene] carbazate: a combined X-ray and density functional theory (DFT) study, Acta Cryst C66 (2010) o353–o355, https://doi.org/10.1107/S0108270110020688.
[37] M.P. Pavan, M.N. Reddy, N.N.B. Kumar, K.C.K. Swamy, Base catalysed synthesis of thiochromans and azo-linked chromenes using allenylphosphonates, Org. Biomol. Chem. 10 (2012) 8113–8118, https://doi.org/10.1039/c2ob26285a.
[38] N.N.B. Kumar, M. Chakravarty, N.S. Kumar, K.V. Sajna, K.C.K. Swamy, Allenylphosphonates with a 1,3,2-dioxaphosphorinane ring: synthesis, structures, stability and utility, J. Chem. Sci. 121 (1) (2009) 23–36, https://doi.org/10.1007/s12039-009-0003-1.
[39] M. Anitha, R. Kotikalapudi, K.C.K Swamy, $FeCl_3$ catalysed regioselective allylation of phenolic substrates with (α-hydroxy)allylphosphonates, J. Chem. Sci. 127 (8) (2015) 1465–1475, https://doi.org/10.1007/s12039-015-0903-1.
[40] M. Chakravarty, K.C.K. Swamy, Palladium-Catalyzed Coupling of Allenylphosphonates, Phenylallenes, and Allenyl Esters: remarkable Salt Effect and Routes to Novel Benzofurans and Isocoumarins, J. Org. Chem. 71 (2006) 9128–9138, https://doi.org/10.1021/jo9901992.
[41] S. Baaziz, N. Bellec, Y.Le Gal, R. Kaoua, F. Camerel, S. Bakhta, B. Nedjar-Kolli, T. Roisnel, V. Dorcet, O. Jeannin, D. Lorcy, Difluoroboron complexes of functionalized dehydroacetic acid: electrochemical and luminescent properties, Tetrahedron. 72 (2016) 464–471, https://doi.org/10.1016/j.tet.2015.11.034.
[42] M. Zhou, Q. Su, Y. Addepalli, Y. He, Z. Wang, An asymmetric Mannich reaction of α-diazocarbonyl compounds and N-sulfonyl cyclic ketimines catalyzed by complexes generated from chiral and achiral phosphines with gold(I), Org. Biomol. Chem. 16 (2018) 2923–2931, https://doi.org/10.1039/c8ob00577j.
[43] F. Bachechi, V.M. Coiro, M. Delfini, N-[2-(1-Hydrazonoethyl)-3-benzofuranyl]-*p*-toluenesulfonamide, Acta Cryst C52 (1996) 2915–2917, https://doi.org/10.1107/S0108270196006968.
[44] J.G. Chang, J. Lu, R.G. Zhao, E,E)-2,5-Bis(5-chloro-2-methoxyphenyl)-3,4-diazahexa-2,4-diene, Acta Crystallogr E 65 (2009) o3185, https://doi.org/10.1107/S1600536809048351.
[45] H. Hopfl, M. Sanchez, N. Farfan, V. Barba, Synthesis and comparative study of three monomeric boronates by spectroscopic methods and X-ray crystallography, Can. J. Chem. 76 (10) (1998) 1853, https://doi.org/10.1139/v98-181.
[46] J.G. Chang, J.K. Li, (*E,E*)-4,4′-Dimethyl-2,2′-(1,1′-dibenzylazino)diphenol, Acta. Cryst. E63 (2007) o4061, https://doi.org/10.1107/S1600536807044182.
[47] M.A. Spackman, D. Jayatilaka, Hirshfeld surface analysis, Cryst. Eng. Comm. 11 (2009) 19–32, https://doi.org/10.1039/B818330A.
[48] P.R. Spackman, M.J. Turner, J.J. Mckinnon, S.K. Wolff, D.J. Grimwood, D. Jayatilaka, M.A. Spackman, CrystalExplorer: a program for Hirshfeld surface analysis, visualization and quantitative analysis of molecular crystals, J. App. Cryst. 54 (2021) 1006–1011, https://doi.org/10.1107/S1600576721002910.
[49] Y.Z. Zheng, Y. Zhou, Q. Liang, D.F. Chen, R. Guo, C.L. Xiong, X.J. Xu, Z.N. Zhang, Z.J. Huang, Solvent effects on the intramolecular hydrogen-bond and anti-oxidative properties of apigenin: a DFT approach, Dyes. Pigm. 141 (2017) 179–187, https://doi.org/10.1016/j.dyepig.2017.02.021.
[50] L. Pauling, The Nature of Chemical Bond third ed, Cornell University Press, New York, 1960.
[51] M. Shebl, M.A. El-ghamry, S.M.E. Khalil, M.A.A. Kishk, Mono- and binuclear copper (II) complexes of new hydrazone ligands derived from 4,6-diacetylresorcinol: synthesis, spectral studies and antimicrobial activity, Spectrochim. Acta A. 126 (2014) 232–241, https://doi.org/10.1016/j.saa.2014.02.014.
[52] M. Shebl, M.A. Ibrahim, S.M.E. Khalil, S.L. Stefan, H. Habib, Binary and ternary copper (II) complexes of a tridentate ONS ligand derived from 2-aminochromone-3 carboxaldehyde and thiosemicarbazide: synthesis, spectral studies and antimicrobial activity, Spectrochim. Acta a 115 (2013) 399–408, https://doi.org/10.1016/j.saa.2013.06.075.
[53] J.A. Mosbo, J.G. Verkade, Dipole moment, nuclear magnetic resonance, and infrared studies of phosphorus configurations and equilibria in 2-R-2-Oxo-l,3,2-dioxaphosphorinanes, J. Org. Chem. 42 (9) (1977) 1549–1555, https://doi.org/10.1021/jo00429a015.
[54] D.M. Gil, Synthesis, molecular structure, spectroscopic and theoretical investigation of 5-chlorosalicylaldehyde-2,4-dinitrophenylhydrazone, J. Mol. Struct. 1205 (2020) 127589, https://doi.org/10.1016/j.molstruc.2019.127589.
[55] W. Arar, A. Khatyr, M. Knorr, L. Brieger, A. Krupp, C. Strohmann, M. L.Efrit, A. Ben Akacha. Synthesis, crystal structures and Hirshfeld analyses of phosphonothioamidates (EtO)2P(=O)C(=S)N(H)R (R = Cy, Bz) and their coordination on CuI and HgX2 (X = Br, I), Phosphorus, Sulfur Silicon. Rel. Elem. 196 (9) 845–858. https://doi.org/10.1080/10426507.2021.1927032.
[56] V. Bertolasi, P. Gilli, V. Ferretti, G. Gilli, K. Vaughan, Interplay between steric and electronic factors in determining the strength of intramolecular resonance-assisted NH…O hydrogen bond in a series of β-ketoarylhydrazones, New J. Chem. 23 (1999) 1261–1267, https://doi.org/10.1039/A906111H.
[57] V. Bertolasi, V. Ferretti, P. Gilli, G. Gilli, B.Y.M. IssaIb, O.E. Sherif, Intramolecular N–H···O hydrogen bonding assisted by resonance. Part 2. Intercorrelation between structural and spectroscopic parameters for five 1,3-diketone arylhydrazones derived from dibenzoylmethane, J. Chem. Soc., Perkin Trans. 2 (1993) 2223–2228, https://doi.org/10.1039/P29930002223.
[58] P. Gilli, V. Bertolasi, V. Ferretti, G. Gilli, Evidence for Intramolecular N-H…O Resonance-Assisted Hydrogen Bonding in *β*-Enaminones and Related Heterodienes. A Combined Crystal-Structural, IR and NMR Spectroscopic, and Quantum-Mechanical Investigation, J. Am. Soc. 122 (2000) 10425, https://doi.org/10.1021/ja000921-10417+.
[59] D. Alonso, I. Dorronsoro, L. Rubio, P. Muñoz, E. García- Palomero, M. Del Monte, A. Bidon-Chanal, M. Orozco, F.J. Luque, A. Castro, M. Medina, A. Martínez, Donepezil-tacrine hybid related derivatives as new dual binding site inhibitors of AChE, Bioorg. Med. Chem. 13 (24) (2005) 6588–6597, https://doi.org/10.1016/j.bmc.2005.09.029.
[60] Y. Ohta, M. Darwish, N. Hishikawa, T. Yamashita, K. Sato, M. Takemoto, K. Abe, Therapeutic effects of drug switching between acetylcholinesterase inhibitors in patients with Alzheimer's disease, Geriatr. Gerontol. Int. 17 (11) (2017) 1843–1848, https://doi.org/10.1111/ggi.12971.

[61] B. Sameem, M. Saeedi, M. Mahdavi, A. Shafiee, A review on tacrine-based scaffolds as multi-target drugs (MTDLs) for Alzheimer's disease, Eur. J. Med. Chem. 128 (2017) 332–345, https://doi.org/10.1016/j.ejmech.2016.10.060.
[62] P.Y. Chiu, C.Y. Wei, Donepezil in the one-year treatment of dementia with Lewy bodies and Alzheimer's disease, J. Neurol. Sci. 381 (2017) 322, https://doi.org/10.1016/j.jns.2017.08.913.
[63] S. Boudriga, S. Haddad, V. Murugaiyah, M. Askri, M. Knorr, C. Strohmann, C. Golz, Three-component access to functionalized spiropyrrolidine heterocyclic scaffolds and their cholinesterase inhibitory activity, Molecules. 25 (8) (2020) 1963–1985, https://doi.org/10.3390/molecules25081963.
[64] A. Akincioglu, E. Kocaman, H. Akıncıoğlu, R.E. Salmas, S. Durdagi, İ. Gülçin, C. T. Supuran, S. Göksu, The synthesis of novel sulfamides derived from β-benzylphenethylamines as acetylcholinesterase, butyrylcholinesterase and carbonic anhydrase enzymes inhibitors, Bioorg. Chem. 74 (2017) 238–250, https://doi.org/10.1016/j.bioorg.2017.08.012.
[65] T. Xu, S. Li, A.J. Li, J. Zhao, S. Sakamuru, W. Huang, M. Xia, R. Huang, Identification of Potent and Selective Acetylcholinesterase/Butyrylcholinesterase Inhibitors by Virtual Screening, J. Chem. Inf. Model. 63 (8) (2023) 2321–2330, https://doi.org/10.1021/acs.jcim.3c00230.
[66] M. Yazdani, N. Edraki, R. Badri, M. Khoshneviszadeh, A. Iraji, O. Firuzi, 5,6-Diphenyl triazine-thiomethyltriazole hybrid as a new Alzheimer's disease modifying agents, Mol. Divers. 24 (2020) 641–654, https://doi.org/10.1007/s11030-019-09970-3.
[67] Q. Li, S. He, Y. Chen, F. Feng, W. Qu, H. Sun, Donepezil-based multi-functional cholinesterase inhibitors for treatment of Alzheimer's disease, Eur. J. Med. Chem. 158 (2018) 463–477, https://doi.org/10.1016/j.ejmech.2018.09.031.
[68] H. Cavdar, M. Senturk, M. Guney, S. Durdagi, G. Kayik, C.T. Supuran, D. Ekinci, Inhibition of acetylcholinesterase and butyrylcholinesterase with uracil derivatives: kinetic and computational studies, J. Enzyme Inhib. Med. Chem. 34 (1) (2019) 429–437, https://doi.org/10.1080/14756366.2018.1543288.
[69] I. Daoud, N. Melkemi, T. Salah, S. Ghalem, Combined QSAR, molecular docking and molecular dynamics study on new Acetylcholinesterase and Butyrylcholinesterase inhibitors, Comput. Biol. Chem. 74 (2018) 304–326, https://doi.org/10.1016/j.compbiolchem.2018.03.021.
[70] M.P. Girard, V. Karimzadegan, M. Héneault, F. Cloutier, G. Bérubé, L. Berthoux, N. Mérindol, I. Desgagné-Penix. Chemical synthesis and biological activities of amaryllidaceae alkaloid norbelladine derivatives and precursors. 27 (17) (2022) 5621–5640. https://doi.org/10.3390/molecules27175621.
[71] O. Trott, A.J. Olson, AutoDock Vina: improving the speed and accuracy of docking with a new scoring function, efficient optimization, and multithreading, J. Comput. Chem. 31 (2010) 455–461, https://doi.org/10.1002/jcc.21334.
[72] A. Imberty, K.D. Hardman, J.P. Carver, S. Perez, Molecular modelling of protein-carbohydrate interactions. Docking of monosaccharides in the binding site of concanavalin A, Glycobiology 1 (6) (1991) 631–642, https://doi.org/10.1093/glycob/1.6.631.
[73] A. Daina, O. Michielin, Zoete V, SwissADME: a free web tool to evaluate pharmacokinetics, drug-likeness and medicinal chemistry friendliness of small molecules, Sci. Rep. 7 (2017) 42717, https://doi.org/10.1038/srep42717.
[74] D.E.V Pires, T.L. Blundell, D.B. Ascher, pkCSM: predicting small-molecule pharmacokinetic and toxicity properties using graph-based signatures, J. Med. Chem. 58 (9) (2015) 4066–4072, https://doi.org/10.1021/acs.jmedchem.5b00104.
[75] C.A. Lipinski, F. Lombardo, B.W. Dominy, P.J. Feeney, Experimental and computational approaches to estimate solubility and permeability in drug discovery and development settings, Adv. Drug Deliv. Rev. 23 (1997) 3–25, https://doi.org/10.1016/s0169-409x(00)00129-0.
[76] D.F. Veber, S.R. Johnson, H.Y. Cheng, B.R. Smith, K.W. Ward, K.D. Kopple, Molecular properties that influence the oral bioavailability of drug candidates, J. Med. Chem. 45 (12) (2002) 2615–2623, https://doi.org/10.1021/jm020017n.
[77] W.J. Egan, K.M. Merz, J.J. Baldwin, Prediction of drug absorption using multivariate statistics, J. Med. Chem. 43 (21) (2000) 3867–3877, https://doi.org/10.1021/jm000292e.
[78] R.B. van Breemen, Y. Li, Caco-2 cell permeability assays to measure drug absorption, Expert. Opin. Drug. Metab. Toxicol. 1 (2) (2005) 175–185, https://doi.org/10.1517/17425255.1.2.175.
[79] Z. Gao, Y. Chen, X. Cai, R. Xu, Predict grug permeability to blood-brain-barrier from clinical phenotypes: drug side effects and drug indications, Bioinformatics. 33 (6) (2017) 901–908, https://doi.org/10.1093/bioinformatics/btw713.
[80] P. Manikandan, S. Nagini, Curr. drug targets. cytochrome P450 structure, Review 19 (2018) 38–54, https://doi.org/10.2174/1389450118666170125144557.
[81] M.J. Frisch, G.W. Trucks, H.B. Schlegel, et al., Gaussian 09. Revision A.1, Gaussian Inc, Wallingford, CT, 2009.
[82] R.D. Dennington, T.A. Keith, J.M. Millam, GaussView 5.0.8, Gaussian Inc, 2008.
[83] A.D. Becke, Density functional thermochemistry. III. The role of exact exchange, J. Chem. Phys. 98 (1993) 1372–1377, https://doi.org/10.1063/1.464913.
[84] Apex 4, Bruker, Bruker AXS Inc, Madison, WI, USA, 2021.
[85] G.M. Sheldrick, A Short History of SHELX, Acta Cryst. A. 64 (2008) 112–122, https://doi.org/10.1107/S0108767307043930.
[86] G.M. Sheldrick, SHELXT – integrated space-group and crystal-structure determination, Acta Cryst. A. 71 (2015) 3–8, https://doi.org/10.1107/S2053273314026370.
[87] G.M. Sheldrick, Crystal Structure Refinement with SHELXL, Acta Cryst. C. 71 (2015) 3–8, https://doi.org/10.1107/S2053229614024218.
[88] O.V. Dolomanov, L.J. Bourhis, R.J. Gildea, J.A.K. Howard, H. Puschmann, OLEX2: a complete structure solution, refinement and analysis program, J. Appl. Cryst. 42 (2009) 339–341, https://doi.org/10.1107/S0021889808042726.
[89] F. Nachon, E. Carletti, C. Ronco, M. Trovaslet, Y. Nicolet, L. Jean, P. Renard, Crystal structures of human cholinesterases in complex with huprine W and tacrine: elements of specificity for anti-Alzheimer's drugs targeting acetyl- and butyryl- cholinesterase, Biochem. J. 453 (2013) 393–399, https://doi.org/10.1042/bj20130013.
[90] J. Cheung, M.J. Rudolph, F. Burshteyn, M.S. Cassidy, E.N. Gary, J. Love, M. C. Franklin, J.J. Height, Structures of human acetylcholinesterase in complex with pharmacologically important ligands, J. Med. Chem. 55 (2012) 10282–10286, https://doi.org/10.1021/jm300871x.
[91] Chemsketch freeware h.t..tps://w.w.w.acdlabs.com/resources/free-chemistry-software-apps/ chemsketch-freeware/, 2023 (accessed 15 March 2023).